INVESTIGATION OF ADVANCED PROPULSION TECHNOLOGIES:

THE RAM ACCELERATOR AND THE FLOWING GAS RADIATION HEATER

NASA Grant No. NAG 1-1288

Final Report

1 July 1991 – 30 June 1992

Prepared by:

A.P. Bruckner
C. Knowlen
A.T. Mattick

Principal Investigators:

A. Hertzberg
A.P. Bruckner
A.T. Mattick

Aerospace and Energetics Research Program
Department of Aeronautics and Astronautics
University of Washington, FL-10
Seattle, WA 98195

ABSTRACT

This report describes work performed for NASA Langley Research Center on advanced propulsion technologies during the time period 1 July 1991 to 30 June 1992. The two principal areas of investigation are the ram accelerator and the flowing gas radiation heater.

The concept of the ram accelerator is presented as a hypervelocity launcher for large-scale aeroballistic range applications in hypersonics and aerothermodynamics research. The ram accelerator is an in-bore ramjet device in which a projectile shaped like the centerbody of a supersonic ramjet is propelled in a stationary tube filled with a tailored combustible gas mixture. Combustion on and behind the projectile generates thrust which accelerates it to very high velocities. The acceleration can be tailored for the "soft launch" of instrumented models. The distinctive reacting flow phenomena that have been observed in the ram accelerator are relevant to the aerothermodynamic processes in airbreathing hypersonic propulsion systems and are useful for validating sophisticated CFD codes. The recently demonstrated scalability of the device, and the ability to control the rate of acceleration offer unique opportunities for the use of the ram accelerator as a large-scale hypersonic ground test facility.

The flowing gas radiation receiver is a novel concept for using solar energy to heat a working fluid for space power or propulsion. Focused solar radiation is absorbed directly in a working gas, rather than by heat transfer through a solid surface. Previous theoretical analysis had demonstrated that radiation trapping reduces energy loss compared to that of blackbody receivers, and enables higher efficiencies and higher peak temperatures. An experiment was carried out to measure the temperature profile of an infrared-active gas, and demonstrate the effect of radiation trapping. This success of this effort validates analytical models of heat transfer in this receiver, and confirms the potential of this approach for achieving high efficiency space power and propulsion.

PREFACE

This research was conducted during the period 1 July 1991 to 30 June 1992 by the Aerospace and Energetics Research Program, University of Washington, Seattle, WA 98195, under Grant No. NAG 1-1288 from NASA Langley Research Center. Dr. Robert Witcofski was the grant monitor.

The authors are deeply indebted to E. Burnham, J. Hinkey, J. Auzias de Turenne, B. Dunmire, G. Chew, and A. Higgins, R. Hoyt, and K. McFall for their assistance in various aspects of this research and for preparing the figures. Thanks are also due to M. Saynor and D. Peterson for their skillful fabrication of the projectiles and to M. Soetrisno of Amtec Engineering, Inc., for permission to reproduce Fig. 11.

TABLE OF CONTENTS

I. THE RAM ACCELERATOR

INTRODUCTION AND OVERVIEW

In recent years there has been a resurgence of interest in hypersonic vehicles and propulsion, and their associated aerothermodynamic phenomena. One example is the National Aerospace Plane (NASP), which is intended to provide easy access to space with the aid of an airbreathing hypersonic propulsion system.[1] Another example is the possible use of aeroassisted orbital maneuvers in the upper atmospheres of Earth and Mars at velocities of 8 to 14 km/sec as a means of reducing the amount of propellant needed to carry out interplanetary missions and thus to reduce costs.[2]

The critical importance of the hypersonic aerodynamic problems attendant to these applications has motivated considerable effort to be directed at developing suitable analytical tools, such as Navier-Stokes CFD algorithms,[3] and experimental facilities, such as hypersonic wind tunnels and ballistic ranges which can provide accurate and scalable data in this difficult to test flight regime.[4,5] The requirement for accurate engineering data requires careful experimentation, preferably in a ground-based facility capable of testing at large scale and at true velocities, with sufficient duration to add confidence to the experimental and computational simulations.

Hypersonic Test Facilities

Historically, four general approaches have been taken in the development of ground-based hypersonic facilities: 1) shock tunnels (both classical shock tube types and gun tunnel or free piston types), in which a high temperature, high pressure shock-heated stagnant gas is expanded through a nozzle to produce high Mach number quasi-steady flow over a stationary model;[6,7] 2) expansion tubes which generate flows over stationary models by means of the non-steady expansion of a moving gas;[8] 3) aeroballistic ranges in which a model launched by a gun-type device flies through a quiescent test gas;[9] and 4) counterflow facilities in which a gun-launched model flies into a counterflowing high speed gas generated by a shock tunnel or expansion tube.[9]

Shock tunnels have been in use since the early 1950's and have generated a very large data base on hypersonic phenomena. However, they have a number of disadvantages, such as spatially non-uniform flow in the test section, limited test duration, and "bruising" and contamination of the test gas, which limit their usefulness. The bruising of the gas is a result of its having to be heated to temperatures above 4000 K to generate flows of sufficient enthalpy to perform high Mach number testing.[10] At such temperatures significant fractions of the test gas are vibrationally excited and dissociated. The nozzle expansion process is so rapid that the some of the gas reaching the test section remains in a non-equilibrium state. The same high temperature stagnation conditions also lead to the formation of nitric oxide in air and can cause nozzle throat erosion, thus contaminating the test gas.[11]

Expansion tubes have been useful for a variety of applications but are prone to non-uniform flow and acoustic disturbances, and are not capable of test times longer than a few hundred microseconds.[8] Experimentation with near full-scale hypersonic components would require very large test sections to minimize wall effects, and extremely long expansion tubes to provide adequate testing times.

Aeroballistic range facilities (of which counterflow facilities are a special case) have been in use for several decades and have provided much useful hypersonic data, typically with small-scale models.[5,9] Aeroballistic ranges do not suffer from the disadvantages associated with accelerating the test gas past a stationary model. In addition, such facilities can, in principle, be designed to provide much longer testing times than shock tunnels or expansion tubes, and offer the possibility of tailoring the conditions of the test gas to more closely match the Mach numbers and Reynolds numbers of interest.

In fairness, it should be mentioned that aeroballistic ranges do pose unique problems of their own, such as the difficulty of instrumenting and accurately tracking a flying model, the need to design acceleration-insensitive models and instrumentation, the problem of data acquisition and telemetry from the hypervelocity model, and the issue of scaling (which is also applicable to shock

tunnel and expansion tube facilities). However, recent developments in launcher and electronics technology have opened the way to circumventing or alleviating these problems, making aeroballistic ranges serious contenders in the quest for hypersonic flow data using sizable models.

Typically, the launcher used in aeroballistic ranges is a two-stage light gas gun, either powder or gas driven.[9] Recently, the Space Systems Division at NASA Langley Research Center has examined the possibility of scaling up the gas gun concept to a very large size, capable of launching models with lateral dimensions of the order of 30-60 cm or more, for the Advanced Hypervelocity Aerophysics Facility (AHAF) concept.[12] Although the gas gun is a mature technology, large scale applications present serious engineering challenges and the test models are subjected to extremely high and non-uniform accelerations.

Electromagnetic railguns and coil guns have also been proposed as hypervelocity model launchers.[12,13] These devices suffer from scaling problems too, particularly as related to the economics and technical problems of electrical energy management and release. Furthermore, they subject the model to intense electromagnetic fields which, if not carefully shielded against, can damage the instrumentation carried onboard the model. In the case of the railgun, extreme accelerations are also a problem.

Ram Accelerator Launchers

A completely different launcher technology called the "ram accelerator" has been under development since 1983 at the University of Washington (UW), for applications as a scalable hypervelocity accelerator capable, in principle, of softly launching projectiles at velocities in excess of 7 km/sec.[14-26] The device (Fig. 1) is based on a ramjet-in-tube concept in which a subcaliber projectile, shaped like the centerbody of a supersonic ramjet, is accelerated in a stationary tube filled with a pressurized mixture of combustible gases, i.e., fuel, oxidizer, and diluent. The projectile itself carries no propellants. Combustion of the propellant mixture is induced by flowfield phenomena associated with the passage of the accelerating projectile. Thus the heat

Conventional Ramjet

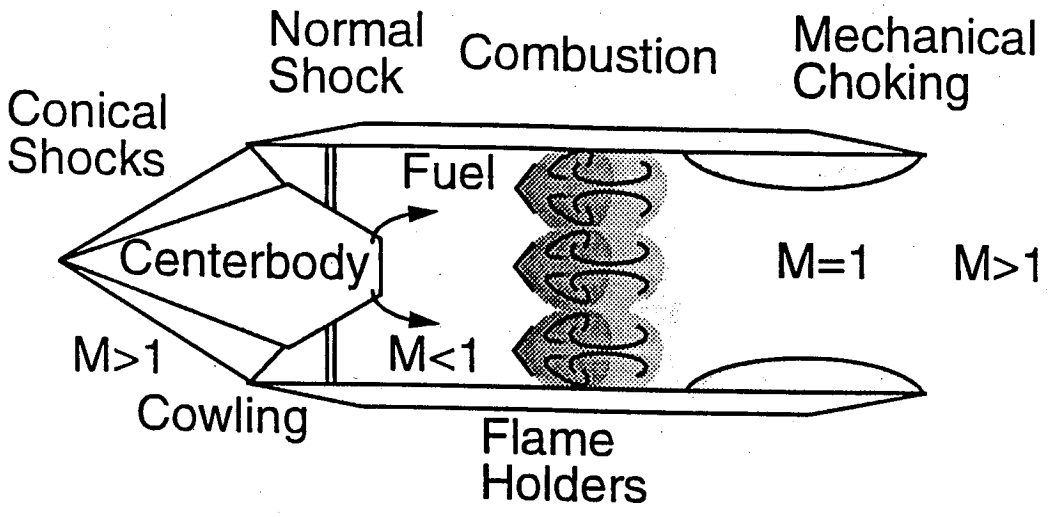

Ram Accelerator

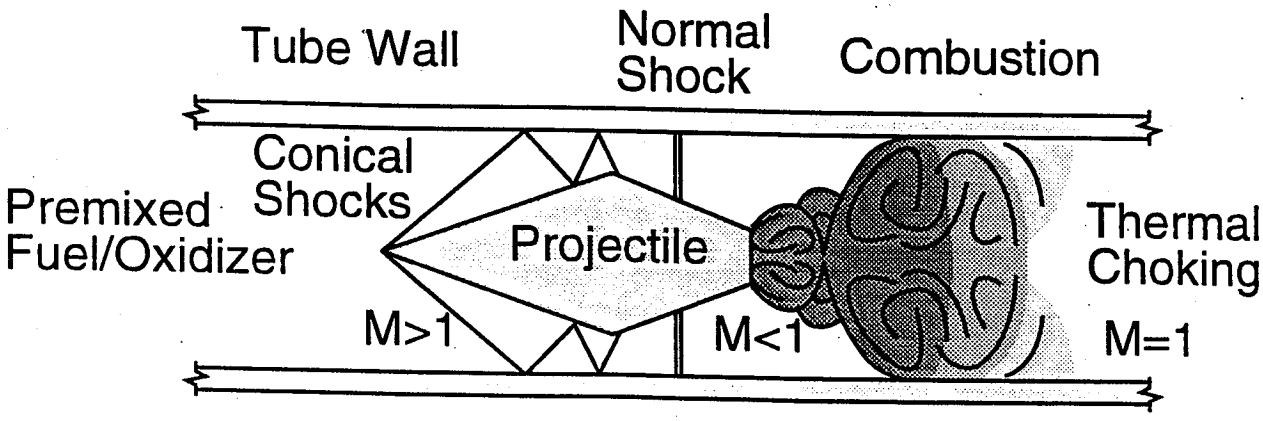

Fig. 1 Schematics of conventional ramjet and ram accelerator.

release process travels with the projectile, generating a pressure distribution which continuously produces thrust. The chemical energy density and speed of sound of the gas mixture can be adjusted, via pressure and composition, to control the Mach number and acceleration history of the projectile.

The nature of the ram accelerator principle owes very little to gun technology. This can be seen by the radical differences in the pressure profiles of a conventional gun and a ram accelerator, as illustrated in Fig. 2. In the ram accelerator the barrel itself is the energy storage device and the projectile accelerates through the energy storage medium, i.e., the propellant gas. The heat release on and immediately behind the projectile result in a traveling pulse of pressure that drives the projectile forward. The highest pressure in the system is always in the vicinity of the projectile's base, rather than at the breech as in a gun. The acceleration is a function of the gas fill pressure and can consequently be easily tailored. Furthermore, the aerothermodynamic cycle of the ram accelerator is independent of size, so that the device can be directly scaled up.

A conventional gun is typically used to impart an initial starting velocity to the projectile (Fig. 3), so that it enters the ram accelerator above Mach 2.5 with respect to the propellant gas.* Since the projectile is aerodynamically unstable in the ram accelerator, some means must be used to keep it centered in the bore. Two approaches are illustrated in Fig. 3: fins on the projectile and rails in the tube. To date fins on the projectile have been used at the UW because of the attendant simplicity of tube fabrication and the greater operational flexibility that this approach offers.

In a constant area tube the ram accelerator propulsive cycle does not generate recoil because the momentum of the rearward moving exhaust gas is equal and opposite to that of the projectile. By properly venting the coupling between the gun and the ram accelerator, both the gun's and the ram accelerator's exhaust gases can be made to emerge as rearward directed jets which largely counteract the recoil of this launching system.

---

* A method for ram accelerating a projectile which is initially stationary has recently been patented by the authors[27] and is briefly described later in this report.

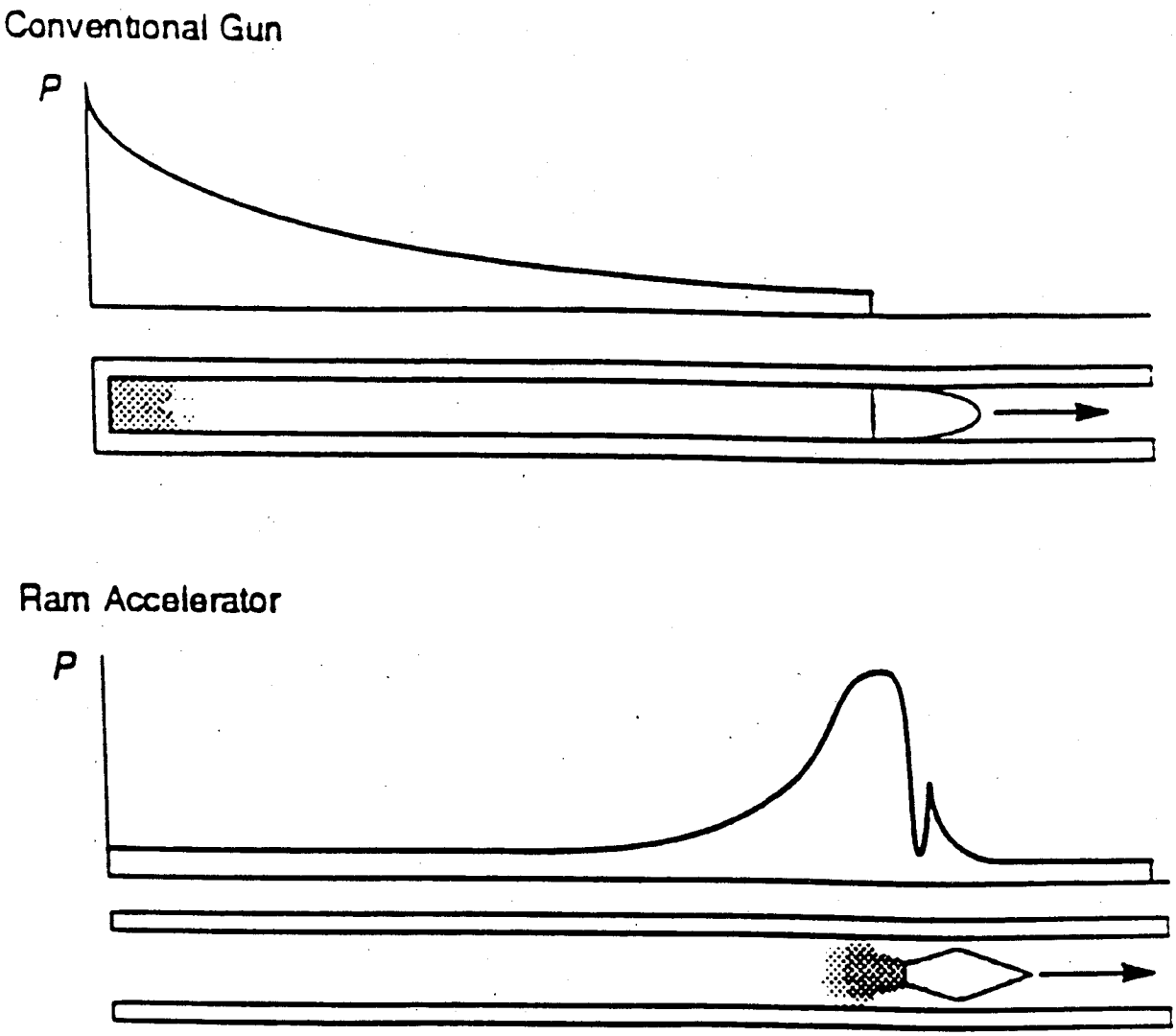

Fig. 2 Characteristic pressure profiles in conventional gun and ram accelerator.

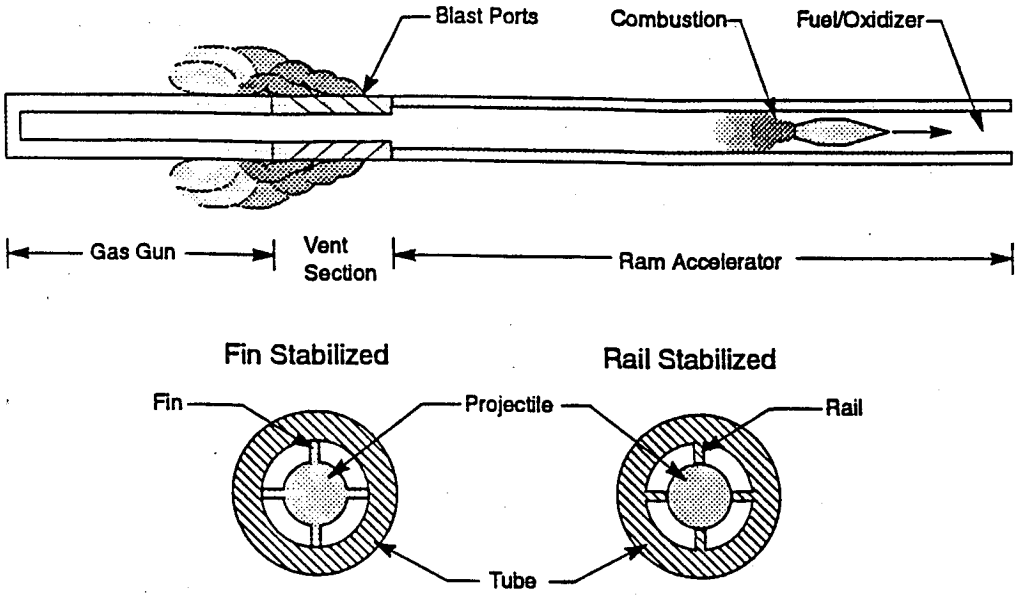

Fig. 3 Ram accelerator with initial launcher.

The ram accelerator concept is operable over a wide range of initial pressures, propellant mixtures, accelerations, and sizes, giving it great potential for ground tests of relatively large, highly instrumented models of hypersonic vehicles over a wide range of conditions.[21,23] The device not only shows promise as a hypervelocity launcher but also as a means to directly investigate hypersonic propulsion cycles of interest to NASP and related vehicles, since these cycles are similar to the propulsive cycles of the ram accelerator itself.

At the University of Washington experiments have been conducted in a 38-mm bore 16-m long ram accelerator using a variety of methane, ethylene, and hydrogen based propellant mixtures, over a wide range of Mach numbers (2.5 to 8.5) and propellant fill pressures (3 to 44 atm). Three different modes of ram accelerator propulsion, centered on the Chapman-Jouguet (C-J) detonation speed of the combustible gas, have been observed. These are the subsonic combustion thermally choked mode,[14,16] observed at "subdetonative" velocities, i.e., below the C-J detonation speed; the "transdetonative" mode,[20] observed to occur at 90% - 110% C-J speed; and the supersonic combustion, "superdetonative" mode[19] in which the projectile is always moving faster than the C-J speed. These distinctive reacting flow phenomena are very useful for validating sophisticated CFD computer codes and in collecting engineering data for potential airbreathing hypersonic propulsion systems.

Related Research Efforts

The potential of the ram accelerator as a test facility uniquely suited for experimental studies of hypersonic flow phenomena has led several groups in the U.S.A. and abroad to become involved in research on this new accelerator concept.[30] The U.S. Army Ballistics Research Laboratory (BRL) has constructed a 120-mm bore ram accelerator to investigate the scaling and other aspects of this technology.[31,32] This device is close to reaching operational status.[33] Preliminary designs of a 93-mm bore facility are currently being developed by the U.S. Air Force at Eglin A.F.B., with intentions to be operational by the end of 1993.[34] At NASA Langley Research Center studies are being performed to assess the potential of the ram accelerator as a

launcher in the AHAF,[12] while CFD studies of the chemically reactive flow in the device are being conducted at NASA Lewis Research Center,[35] the Naval Research Laboratory,[36] and SAIC.[34] Related work is being carried out by Amtec Engineering, Inc., which is modeling ram accelerator flowfields to demonstrate the capabilities of its CFD codes,[37] and by Advanced Projects Research, Inc. (APRI) which has conducted exploratory experiments in a 38-mm bore test facility under Small Business Innovative Research funding.[38]

In France, researchers at the Institut Franco-Allemand de Recherches de St. Louis (ISL) have constructed a 90-mm bore ram accelerator and have recently succeeded in demonstrating its operation, thus becoming the second research institute in the world with a fully operational ram accelerator.[39] Their work has confirmed the feasibility of scaling up the concept. In addition, researchers at ISL have completed a 38-mm device with in-bore rails that mates with a conventional 30-mm bore powder gun.[40] Preliminary tests are expected to begin in the later half of 1992.

In this report we briefly review the ram accelerator propulsion modes that have been observed, and discuss their relevance to hypersonic propulsion cycles. We also present a discussion of the proposed use of the ram accelerator as a launcher for a large-scale hypersonic aeroballistic range facility. Specific examples of 30 cm and 60 cm bore devices are included. Finally, we discuss the engineering issues which need to be addressed in order to develop a large-scale aeroballistic test facility based on the ram accelerator principle.

RAM ACCELERATOR PROPULSION MODES

Several different ram accelerator propulsion modes (Fig. 4) have been identified which are distinguished by the manner in which combustion is stabilized and by their corresponding Mach number and velocity regimes of operation.[16,19,20,22] The propulsive cycle having the lowest operating velocity and Mach number is the thermally choked mode (Fig. 4a).[16] It operates at velocities below the Chapman-Jouguet (C-J) detonation speed of the propellant gas, i.e., in the "subdetonative" velocity regime, with in-tube Mach numbers typically ranging from 2.5 to 4. In

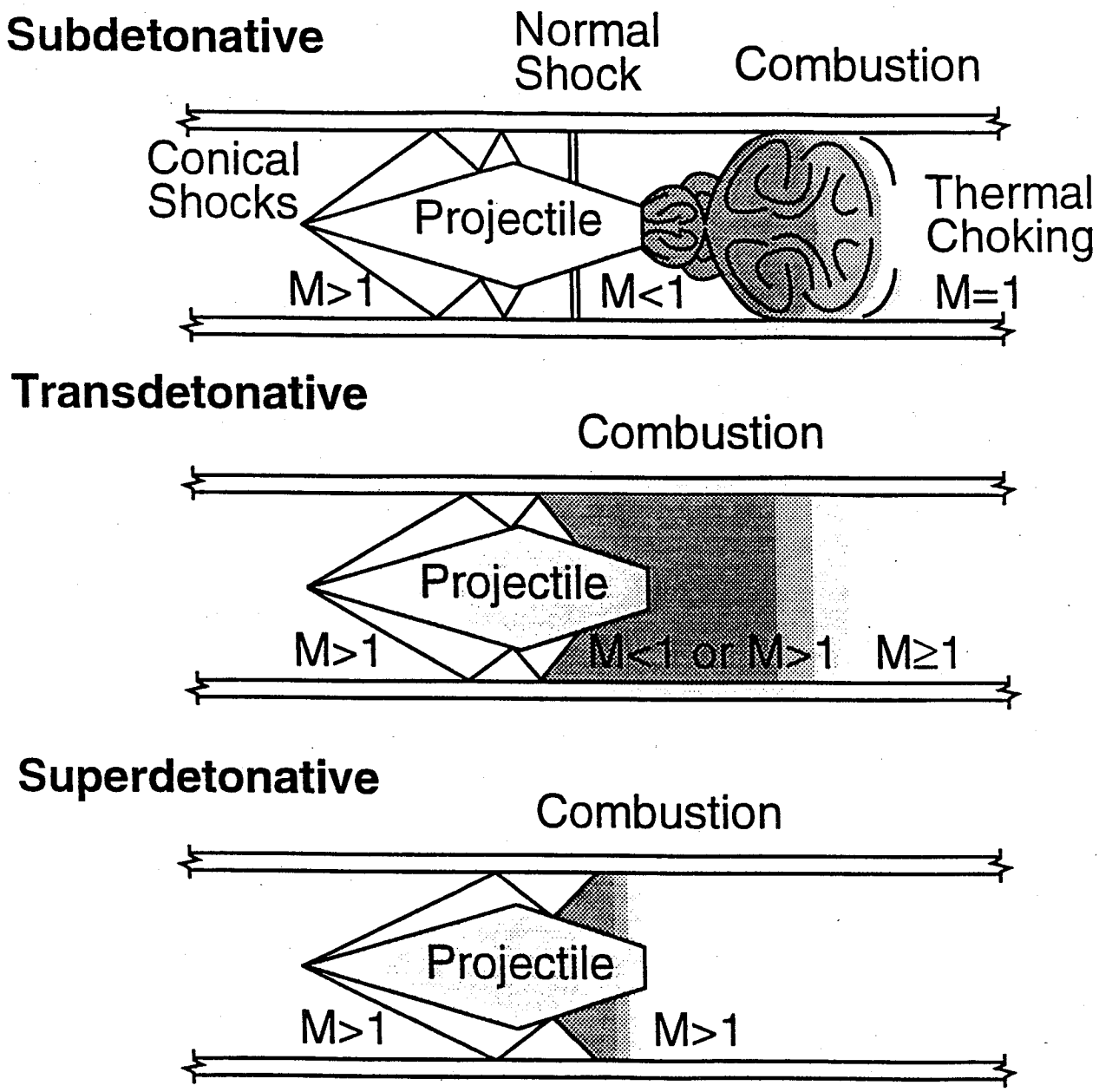

Fig. 4 Ram accelerator propulsive modes.

this mode the thrust is provided by the high base pressure resulting from a normal shock system that is established on the rear half of the projectile body. This shock system is stabilized by thermally choked subsonic combustion behind the projectile.[14,16] Theoretically, this complicated shock system is represented with an ideal normal shock that recedes along the body as the Mach number increases. In the hypothetical case where the projectile tail tapers to a point and the flow is inviscid, the normal shock gradually falls back to the full tube area. A normal shock in a constant area duct followed by heat addition and thermal choking, under steady flow conditions, is a C-J detonation wave. Thus, one-dimensional theory predicts that the thrust goes to zero as the projectile velocity approaches the C-J detonation speed of the propellant mixture. For velocities below 90% of the C-J speed, the ram accelerator thrust as a function of Mach number has been found to be accurately predicted by the 1-D theoretical model of the thermally choked propulsive mode.[41]

At velocities above 90% C-J speed, however, the observed thrust typically begins to exceed the predicted thrust, to the extent that the acceleration increases with increasing velocity as the projectile reaches the C-J speed.[20,22] This anomalous result (in the context of thermally choked theory) coincides with the experimental observation of combustion activity occurring on the projectile body. Indicated in Fig. 4b are generalized heat addition regions, located on and behind the projectile, which may contribute to the overall thrust at velocities near the propellant's C-J speed. Experiments have demonstrated that in the "transdetonative" velocity regime (typically Mach 4 to 6) projectiles can accelerate smoothly from below to above the C-J speed of the gaseous propellant.

For accelerating projectiles at in-tube Mach numbers greater than 6, several "superdetonative" propulsive modes have been investigated both theoretically and experimentally.[15,17-19,22] These propulsive cycles use various supersonic combustion mechanisms to generate thrust at velocities greater than the C-J speed of the propellant gas. One proposed supersonic combustion process involves shock-induced combustion, wherein the

propellant mixture is ignited by one of several reflected shock waves, as shown in Fig. 4c.[17,18] The supersonic heat release raises the gas pressure on the rear half of the projectile, resulting in substantial thrust as the reacted propellant expands back to full tube area. Other combustion processes capable of accelerating projectiles at superdetonative velocities have also been suggested, such as oblique detonation wave[15] and mixed-mode combustion cycles (e.g., heat addition processes that occur in both subsonic and supersonic regions of the flowfield). The oblique detonation wave ram accelerator propulsive cycle is similar to that proposed for the oblique detonation wave engine.[42,43]

EXPERIMENTAL FACILITY

The University of Washington ram accelerator facility (Fig. 5) consists of a light gas gun, light gas dump tank, ram accelerator section, final dump tank, and projectile decelerator.[28] The 38-mm bore, 6-m long, single-stage light gas gun is capable of launching the obturator and projectile combination (typical combined mass approximately 60 to 100 g) to speeds up to 1300 m/s. The muzzle of the gas gun is connected to a perforated tube that passes through an evacuated tank, which serves as a dump for the helium driver gas.

The 16-m long ram accelerator section consists of eight steel tubes, with a bore of 38 mm and an outer diameter of 102 mm. There are a total of 144 instrumentation ports at 40 axial locations, spaced at 40 cm intervals along the accelerator tube. At 24 axial stations there are four orthogonal ports, and at 16 stations there are three ports separated by 120°. This permits the use of either three or four transducers at each station. Piezoelectric pressure transducers, electromagnetic transducers,[44] and fiber-optic light guides[45] can be located in any of these observation stations. A 32-channel, 1-MHz digital data acquisition system is used to record the data. Multiplexing permits monitoring more than 100 separate input signals.

The ram accelerator tube is designed to operate at propellant fill pressures up to 50 atm. Thin Mylar diaphragms are used to close off each end of the accelerator tube and to separate

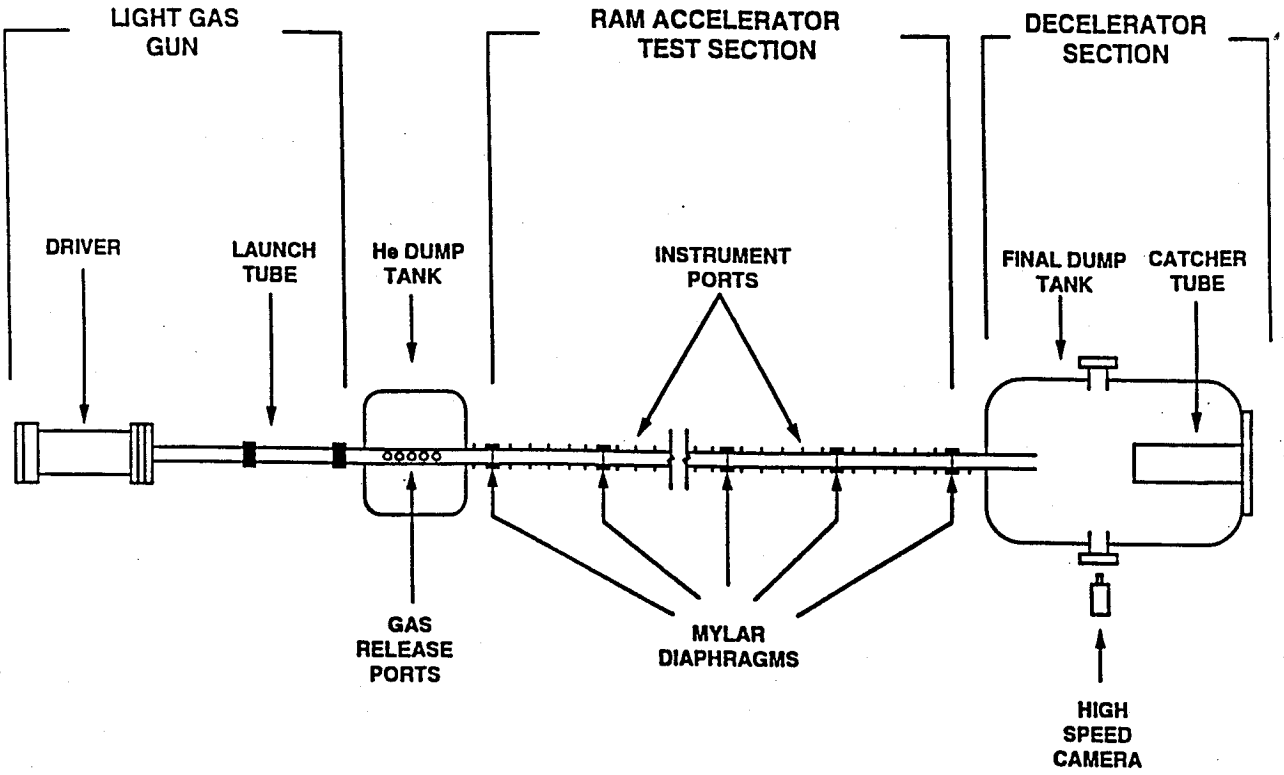

Fig. 5 University of Washington ram accelerator facility.

sections of the tube filled with different propellant mixtures. Steady mass flow rates of the fuel, oxidizer, and diluent gases are maintained during the loading procedure by regulating the pressures upstream of the sonic orifices. The individual streams of gas are brought together downstream of the orifices to mix in the high pressure tubing that routes the propellant mixture to the appropriate sections of the ram accelerator tube.

The end of the ram accelerator test section is connected by a 0.76-m long drift tube to a 2.4-m long evacuated dump tank, through which the projectile flies unconstrained. The tank has a pair of 25-cm diameter viewing ports used for high-speed photography. The free-flying projectile impacts a metal witness plate and is brought to a stop in carpet remnants that are tightly packed in a 20-cm bore x 1-m long tube, which protrudes inside the final dump tank and is attached to the end wall (Fig. 5).

The basic projectile geometry that has been used in the majority of the experimental work to date is illustrated in Fig. 6. It is fabricated of either magnesium alloy or aluminum alloy in two hollow pieces, the nose cone and the body, which are threaded together. Projectiles have ranged in mass between 45 and 90 g, depending on the choice of material and structural details. The fins serve to center the projectile in the tube, and the octagonal cross section of the body is simply a machining convenience. Thin magnetic disks are mounted in the nose-body joint and in the base of the body. When the projectile passes by the electromagnetic transducers in the accelerator tube, the magnets induce signals that are used to determine the time-distance (t-x) history of the projectile and, thus, its velocity and acceleration.

The obturator (Fig. 6), which is used both to seal the barrel of the initial gas gun and to ignite the propellant gas in the ram accelerator,[29] is fabricated from polycarbonate (Lexan) and consists of two pieces with a combined mass of 15 g. The main body has a length to diameter ratio of 0.42 and is perforated axially with a series of regularly spaced holes whose total cross-sectional area is approximately 40% of that of the tube. A thin flat plate of the same material is used to seal these perforations against the driving gas in the light gas gun. This plate is snugly

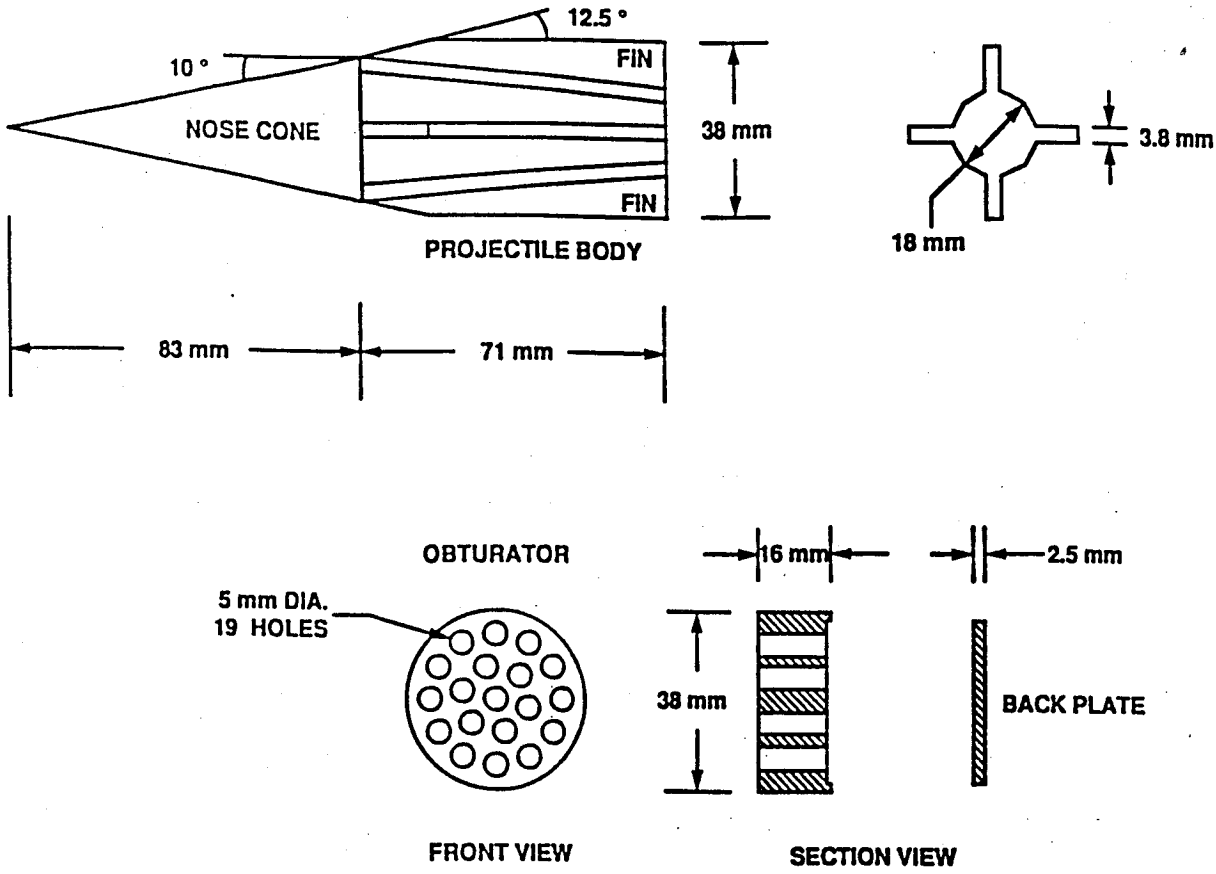

Fig. 6 Experimental ram accelerator projectile and obturator.

fitted into a shallow cavity machined in the back of the main body of the obturator. When the obturator and projectile combination pierces the first diaphragm and enters the propellant mixture, the interaction of the obturator with the gas drives a normal shock onto the projectile body, generating a subsonic flow region behind the projectile. This interaction also heats the gas between the projectile base and the obturator sufficiently to ignite it. The back plate is dislodged by the high frontal pressure on the obturator; this allows reacted gas to flow through the obturator, weakening the normal shock sufficiently to prevent it from outrunning the projectile. Within the first meter of the ram accelerator test section the obturator falls far enough behind the projectile that thermal choking is achieved, thus gasdynamically decoupling the projectile from the obturator.

EXPERIMENTAL RESULTS

Thermally Choked Mode

Experiments to date on the thermally choked mode have been carried out with a variety of propellant mixtures using methane, ethylene, and hydrogen as the fuels, and oxygen as the oxidizer. Diluents such as carbon dioxide, nitrogen, argon, helium, excess methane, and excess hydrogen are used to adjust the acoustic speed of the mixtures so that the initial Mach number of the projectile exceeds the minimum required to start the diffuser, and to tailor the heat release of combustion to a level that assures reliable ignition while reducing the likelihood of a premature detonation.

Figure 7 displays typical transducer signals obtained in a thermally choked ram accelerator. The time intervals are shown in increments of 60 msec and pressure is shown in units of atmospheres. The fill pressure was 40 atm, the projectile's in-tube Mach number was 3.6, and the propellant mixture consisted of $2.7CH_4 + 2O_2 + 5.6N_2$. The upper trace displays the output of an electromagnetic (EM) transducer located at the same axial station as the pressure transducer and fiber-optic probe. The zero crossing of the signal identifies the point in time at which the annular magnetic disk located at the projectile throat (the point of maximum projectile diameter) passes by

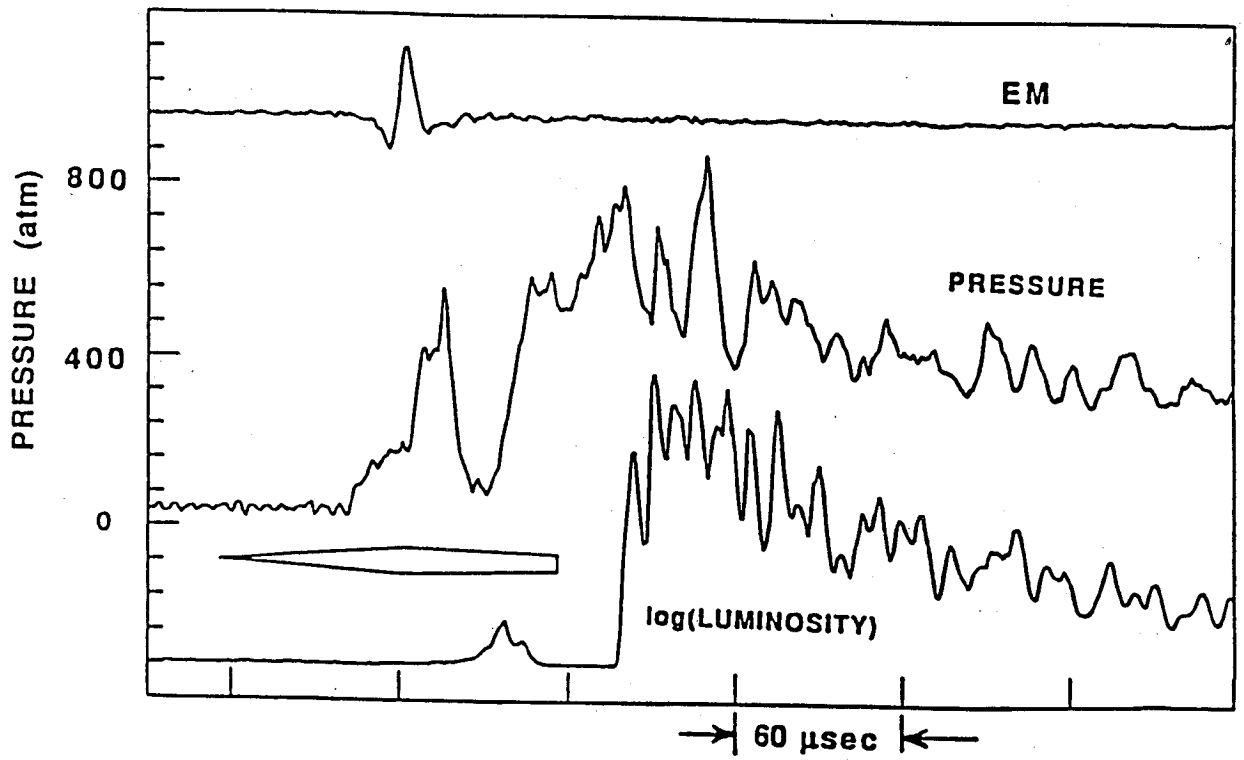

Fig. 7 Typical electromagnetic (EM), pressure, and luminosity signals from the thermally choked propulsive mode of the ram accelerator.

the sensor. This signal provides a reference point from which the position of the shock system can be determined relative to the projectile. A profile of the projectile, with its length scaled to the local velocity, is also shown with its throat aligned with the EM signal.

The middle trace in Fig. 7 is a typical tube wall pressure profile for the thermally choked operating mode. The first abrupt rise in pressure is generated by the lead conical shock and its reflection; subsequently, the pressure rises gradually until the shock reflecting off the nose cone strikes the tube wall again, in the throat region of the projectile diffuser section. Several more reflected shocks are observed in the region of supersonic flow over the projectile body. A normal shock system follows on the rear half of the projectile, producing a high base pressure. This shock system, which is believed to consist of a complex series of oblique and normal shocks, decelerates the flow entering the combustion zone to a subsonic Mach number. The decay in pressure following the peak is consistent with the assumption of subsonic heat addition (which accelerates the flow to thermal choking) and the subsequent non-steady expansion of the combustion products behind the choke point.

The bottom trace in Fig. 7 shows the output from a fiber-optic probe located at the same station as the pressure and electromagnetic probes. The fiber-optic probes are used to examine broadband light emitted as the projectile and chemically reacting gas pass by the instrument stations. Light intensity is logarithmically amplified to enable monitoring of the weak luminosity observed in the shock waves and the intense light emissions associated with combustion. The luminosity trace peaks approximately one projectile length behind the base of the projectile in the region of decaying pressure. This observation is typical of low Mach number ($M<4$) operation in most of the propellant mixtures investigated to date, indicating that the combustion reactions are completed within one to two projectile lengths behind the projectile.

Velocities up to 2650 m/s have been attained with the thermally choked mode of propulsion. An example of the velocity-distance (v-x) profile for a thermally choked experiment is shown in Fig. 8. This experiment was conducted with a four-stage configuration in which the

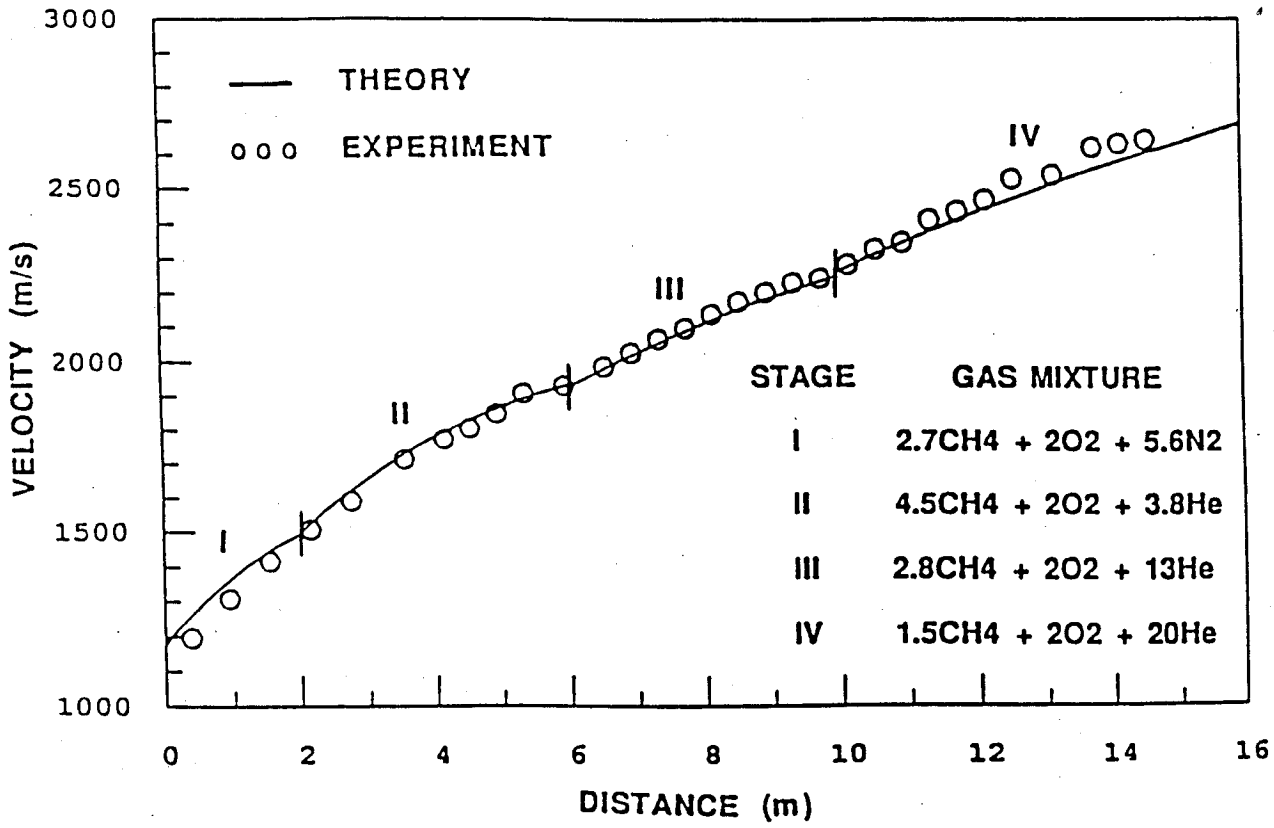

Fig. 8 Velocity-distance record of thermally choked ram accelerator using four stages.

first three stages were filled to approximately 40 atm and the fourth stage to 33 atm. The ram accelerator tube was loaded with successive combustible gas mixtures whose acoustic speeds increased towards the muzzle. The compositions of the propellant mixtures are tabulated in Fig. 8. In this manner the projectile Mach number was kept within relatively narrow limits (approximately 3 - 4) in each stage. The projectile mass was 68 g and its geometry was the same as that shown in Fig. 6. The entrance velocity to the first stage was 1175 m/s and the peak velocity of the experiment occurred ~15 m down the tube at a velocity of 2650 m/s. The normal shock system was then disgorged over the nose of the projectile and the "unstarted" projectile decelerated. The solid curves in the figure represent the theoretical performance predicted by the one-dimensional thermally choked model. Close agreement between theory and experiment is demonstrated for all four propellant mixtures, supporting the assumption that the projectile was accelerated by a thermally choked propulsive cycle.

It has been observed occasionally that the projectile will unstart at high speeds before it reaches the C-J detonation speed of propellant mixtures containing over 60% helium by volume. These mixtures have high acoustic and C-J speeds, which consequently result in relatively low Mach number (M<4) unstarts. By themselves, these low Mach number unstarts are very puzzling because the projectiles operate very well up to Mach 6 in the mixtures having nitrogen and methane as the diluents. One of the primary differences between the experiments in the helium-diluted mixtures and the others is the relatively long duration of acceleration through pressurized propellant gas, resulting in very high projectile velocities (typically above 2300 m/s) by the time it enters the helium-diluted mixture. Thus, the interaction of the projectile fins with the tube wall is expected to be significant, and the performance may be very sensitive to fin erosion. Another key difference between these experiments is that the ratio of specific heats of the helium-diluted mixtures is higher than that of the nitrogen- and methane-diluted mixtures, resulting in greater static temperature rises through the shock system around the projectile when it is operating at the same Mach number in the helium-diluted mixtures. Thus, pre-ignition of the propellant is more likely to occur at lower Mach numbers in the helium-diluted mixtures.

Transdetonative Regime

The transdetonative propulsion mode is an unexpected and very significant finding which grew out of experiments on the thermally choked mode at velocities approaching the C-J detonation speeds of various test mixtures.[20] These results show that acceleration of the projectile exceeds the acceleration expected from thermally choked operation when projectile velocities exceed about 90% of C-J speed. This phenomenon is reproducible and occurs in many of the propellant mixtures investigated to date.[22]

Since the ram accelerator can propel projectiles continuously through the propellant mixture, a single-stage experiment allows study of the development of the flow around the projectile as it operates through a wide range of Mach numbers.[20] Figure 9 shows representative pressure and luminosity data obtained in a single-stage experiment, in a gas mixture of $2.5CH_4 + 2O_2 + 5.5N_2$ at a fill pressure of 31 atm. This propellant mixture has a theoretical C-J detonation velocity of 1770 m/s. In this experiment the 73 g projectile entered the ram accelerator at 1170 m/s and reached a peak velocity of 2070 m/s.

The transdetonative mode differs from the subdetonative mode in that the flow ceases to be thermally choked at full tube area behind the projectile and some of the heat addition appears to occur on the projectile body. This hypothesis is supported by data from the fiber-optic probes, which show the region of intense luminosity moving forward onto the rear of the projectile at the higher Mach number end of the thermally choked operation range. The pair of traces shown in Fig. 9 is from a fiber-optic probe (upper trace) and a pressure transducer (lower trace) located 4.8 m into the ram accelerator tube, where the projectile velocity and Mach number are 1755 m/s and 4.8, respectively (99% of C-J speed). The pressure is seen to rise on the rear half of the projectile and the peak pressure is approximately 600 atm. The light emission data show that light is emitted from both the projectile body and a region extending behind the projectile base. There is also a large spike in luminosity at the projectile throat. It is uncertain if the dip in the luminosity

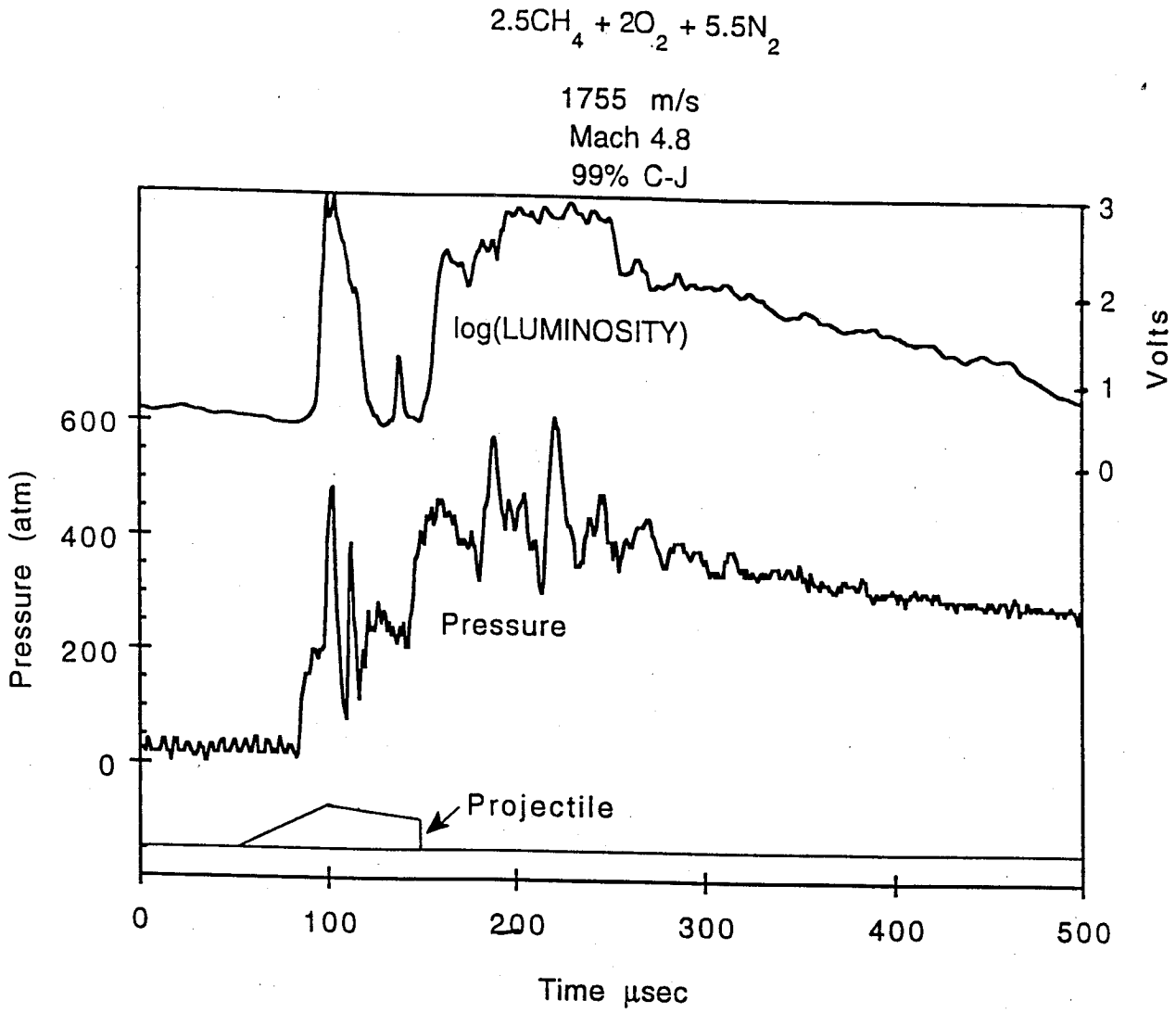

Fig. 9 Pressure and luminosity signals from the transdetonative propulsive mode.

trace over the rear half of the projectile indicates a region of low intensity light or dimming due to fin orientation with respect to the sensor.

The performance characteristics of different propellant mixtures can be compared using a non-dimensional thrust coefficient, I = F/(pA), where F is the ratio of the experimentally determined thrust, p is the propellant fill pressure, and A is the tube cross-sectional area.[14,16,41] The data in Fig. 10 show the variation of thrust coefficient with projectile velocity (normalized to the C-J detonation speed of the propellant mixture) in the experiment discussed above. Projectile acceleration, and hence thrust, was determined by differentiating a polynomial curve fit to the v-x data, which was obtained by center differencing the original t-x data. The order of the polynomial was chosen to minimize the standard deviation in projectile velocity. The solid curve in Fig. 10 is the thrust coefficient profile predicted by the one-dimensional thermally choked model.

The experimental thrust coefficient follows the theoretical prediction very well up to 90% C-J detonation speed. The thrust reaches a relative minimum at about 95% C-J speed and then increases with increasing projectile velocity, reaching a relative maximum at approximately 108% C-J speed in the present case. It is believed that near the thrust minimum the projectile undergoes a transition from the thermally choked propulsive mode. Other propellant mixtures have shown similar behavior in the upward trend of the thrust coefficient, indicating that the transdetonative propulsive mode can be exploited in many gas mixtures.[20,22] The experimental demonstration of transdetonative propulsion confirms that a ram accelerator projectile can be operated over a wide Mach number range, from subdetonative to superdetonative velocities, all within a single propellant mixture.

The mechanism by which heat is released during transdetonative operation is believed to involve both subsonic and supersonic combustion. Recent CFD modeling by Soetrisno and Imlay[37] appears to bear this out. Figure 11 shows a series of pressure contour plots in the vicinity of the projectile at various velocities, both below and above the C-J detonation speed in a propellant mixture similar to that of Fig. 9. At 81% C-J speed the pressure contours show typical

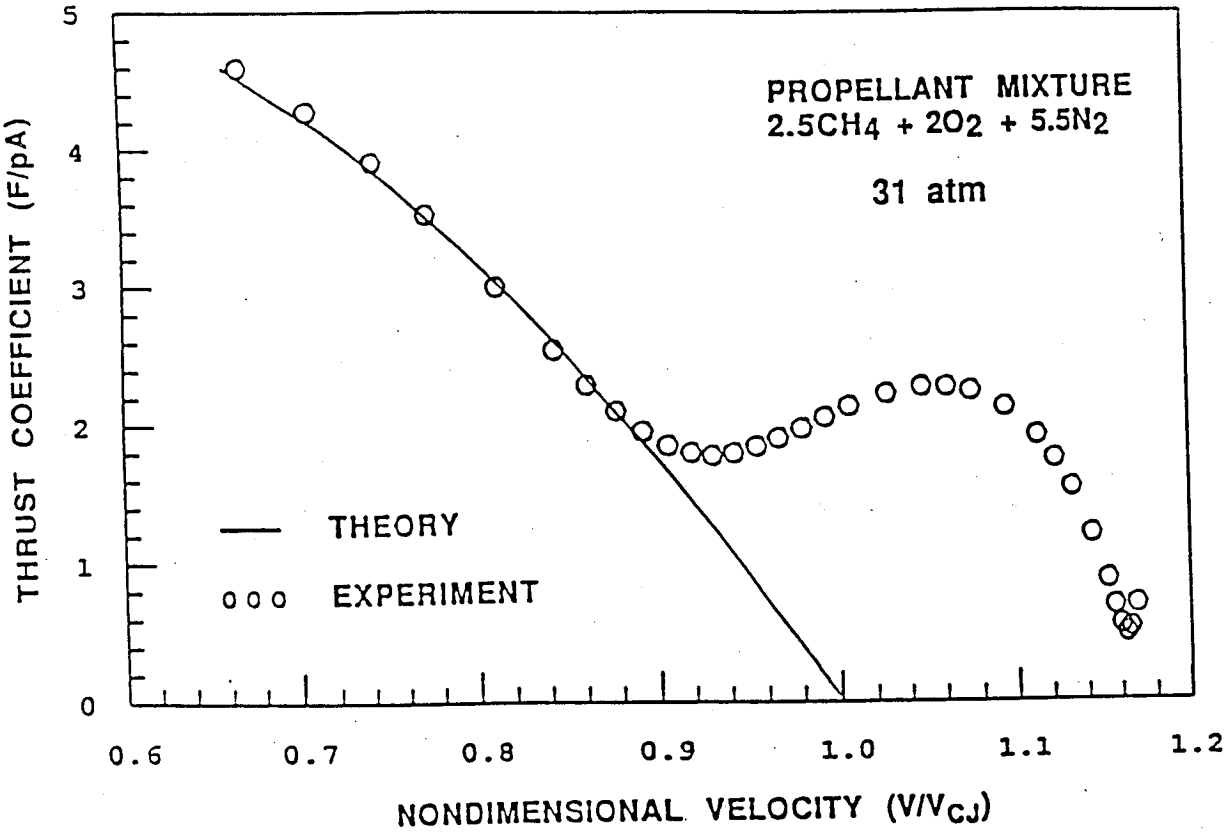

Fig. 10 Nondimensional thrust vs. fraction of CJ speed predicted by theory for thermally choked propulsive mode compared to experiment.

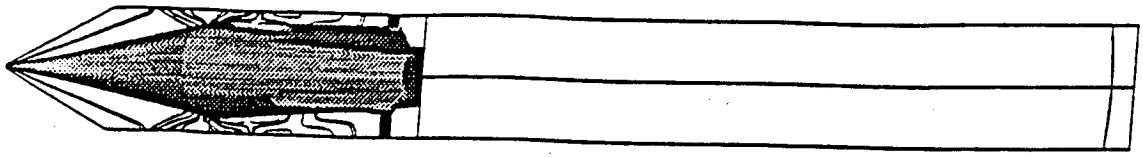

Pressure Contours ($V/CJ = 0.81$)

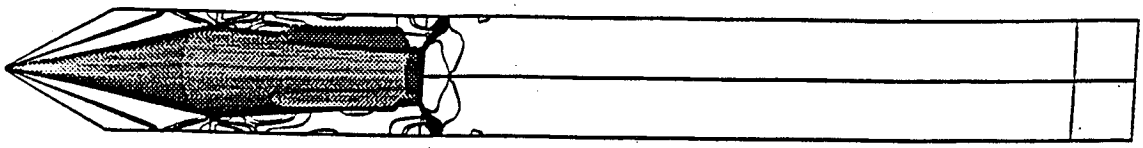

Pressure Contours ($V/CJ = 0.90$)

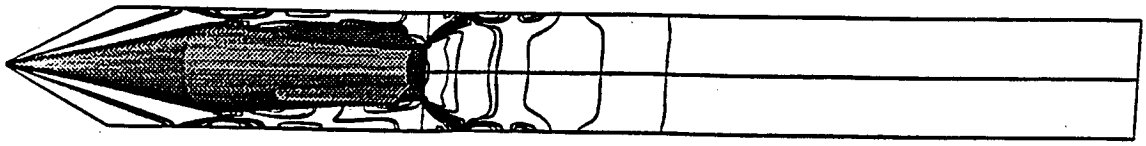

Pressure Contours ($V/CJ = 1.05$)

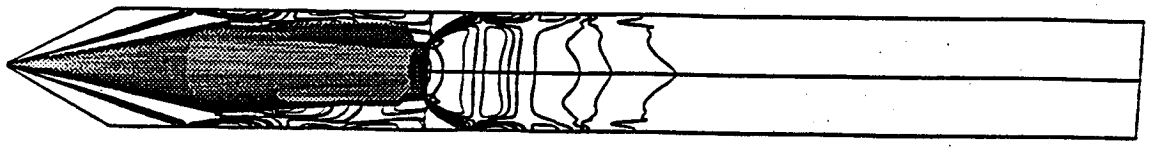

Pressure Contours ($V/CJ = 1.16$)

Fig. 11 Pressure contours in transdetonative velocity regime from axisymmetric CFD model.[37]

thermally choked operation, with a normal shock on the projectile body. At 90% C-J speed the normal shock has become an oblique shock attached to the projectile's base. This shock becomes more oblique as the velocity of the projectile increases. Since this shock is no longer normal, it is not sufficient to render the flow behind it subsonic over the entire domain. Thus, behind the oblique shock there is a region of mixed flow in which part of the combustion occurs supersonically and the rest subsonically.

In Fig. 9, as noted above, the luminosity on the body of the projectile indicates that there is also combustion occurring on the projectile itself. The ignition of the propellant flow on the body may be shock-induced or caused by shock-boundary layer interactions. There is also evidence indicating that magnesium projectiles have a tendency to experience extraordinary accelerations (in the context of the thermally choked theory) at lower velocities than aluminum projectiles,[45,46] leading to the hypothesis that the projectile material may be involved in the chemistry of combustion under certain conditions.

Superdetonative Regime

The experimental thrust coefficient (Fig. 10) in the nitrogen-diluted propellant mixture peaks at a velocity approximately 8% greater than C-J speed and then decreases rapidly with increasing velocity. This roll-over of the thrust coefficient has been seen in several experiments with methane-based propellant mixtures when the projectile has reached velocities over 110% C-J detonation speed.[22] Figure 12 shows transducer signals obtained from the same experiment as the data shown in Fig. 9 but at a velocity well above the C-J detonation speed. The pair of traces show data from an instrument station located 11.8 m into the tube, where the projectile velocity is 2015 m/s (Mach 5.6; 113% C-J speed). The peak pressure is approximately 500 atm, and the character of the tube-wall pressure profiles is similar to that shown in Fig. 9.

The light emission data show considerable luminosity on the nose of the projectile, probably as a result of ignition at the stagnation point of the nose and in the boundary layer. The

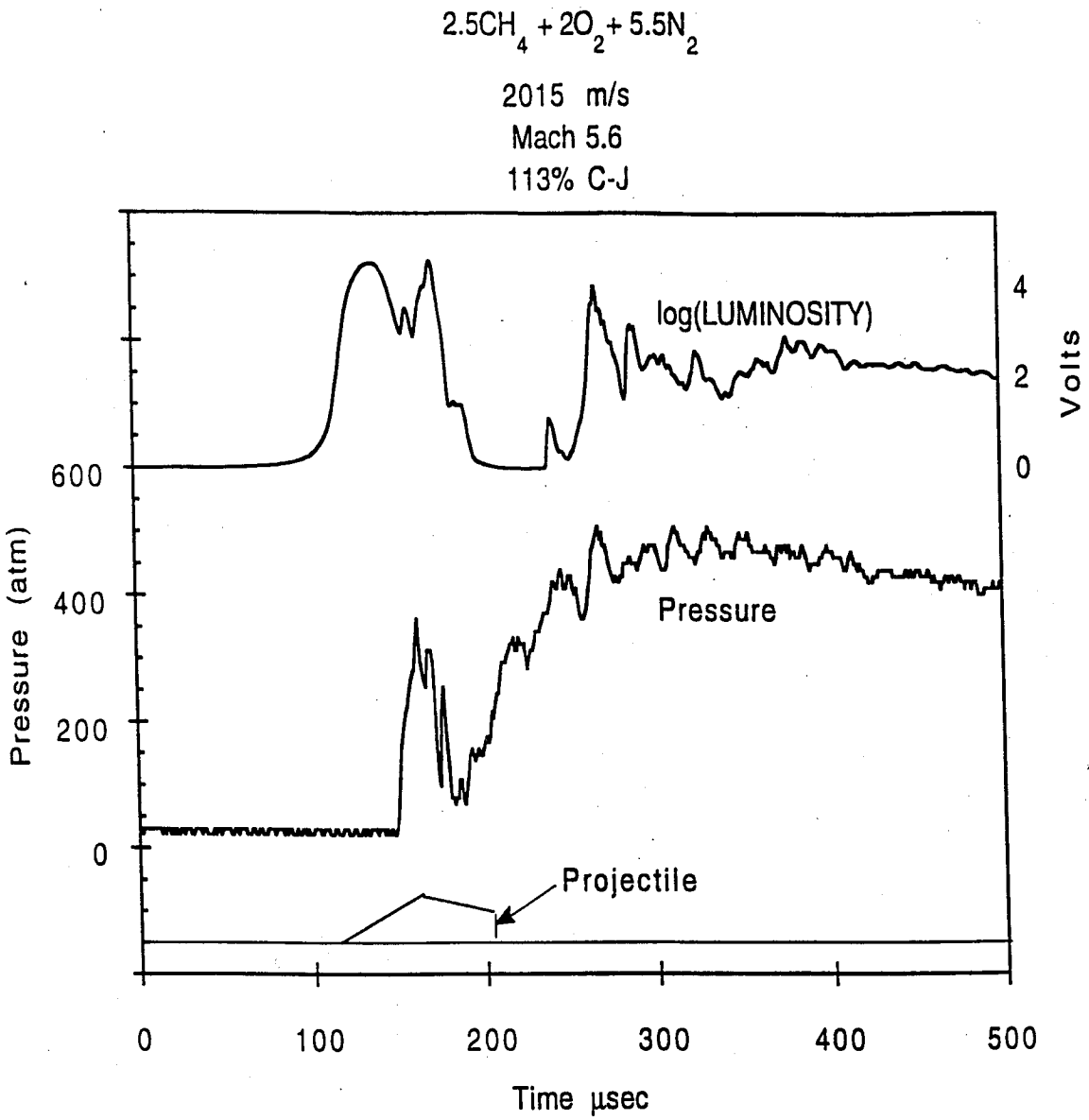

Fig. 12 Pressure and luminosity signals from superdetonative propulsive mode.

combustion in the boundary layer propagates into the free stream at the laminar flame speed, which is much less than the velocity of the free stream relative to the projectile; thus, this mechanism generates only a thin layer of preburned gas ahead of the throat. However, the combustion initiated at the stagnation point produces an entropy layer which may encompass a larger fraction of the flow around the projectile, especially at higher Mach numbers.[47] The pre-ignition of some propellant gas ahead of the throat causes an increase in drag which counteracts the thrust resulting from expansion of the supersonic combustion products over the body of the projectile.[18,47] This effect may be responsible for the decrease in thrust coefficient above about 110% C-J detonation speed.

Experiments were also performed in which projectiles operating in the thermally choked mode and travelling at 2000-2200 m/s abruptly entered a stage containing an ethylene-based propellant mixture, $0.9C_2H_4 + 3O_2 + 5CO_2$, which has an experimentally measured C-J detonation speed of 1650 m/s at 16 atm.[15] The projectiles thus entered the final mixture at velocities 20-30% higher than the C-J speed.

Figure 13 displays the outputs from a pressure transducer and a light emission probe located 0.2 m beyond the entrance of the test stage. (The luminosity signal was linearly amplified in this case, in contrast to the logarithmic amplification shown in Figs. 7 and 9). The projectile velocity and Mach number are 2040 m/s and 7.0, respectively (124% C-J speed). The pressure trace exhibits a series of reflected shocks of increasing amplitude, one of which correlates with the second peak of the light emission profile, possibly indicating the presence of an oblique detonation wave. There is also considerable light emission from the nose of the projectile, indicating pre-ignition ahead of the throat, as in Fig. 12. These data suggest that combustion occurs mainly on the projectile body in contrast to the thermally choked mode, where all combustion activity occurs behind the projectile. The small amount of light emission behind the projectile in Fig. 13 may be a result of recombination or the formation of carbon particles (soot). The projectile was observed to accelerate in this propellant mixture up to 2480 m/s, i.e., 150% C-J speed. The peak Mach

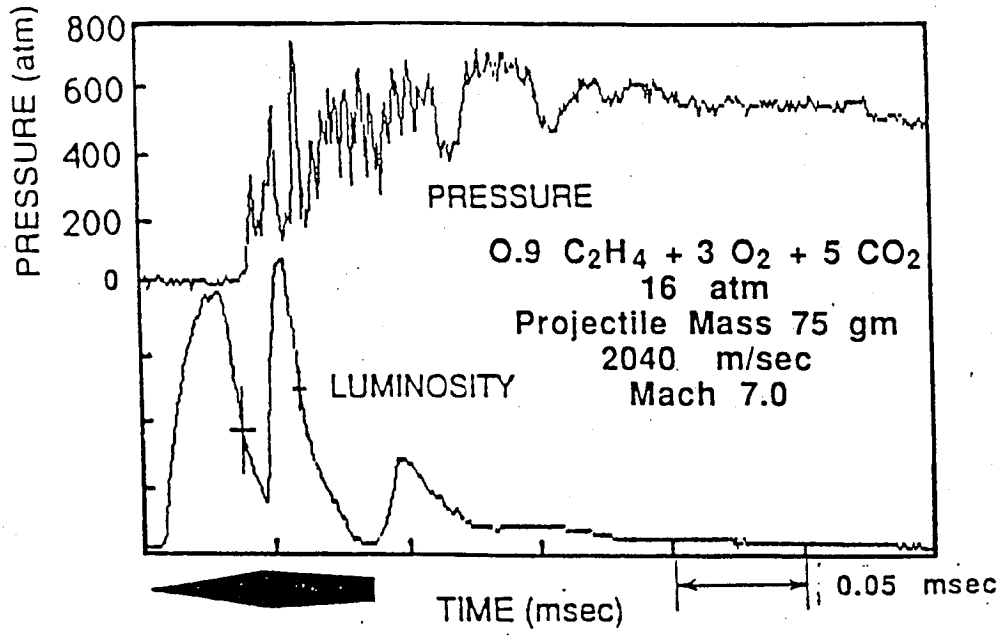

Fig. 13 Pressure and luminosity signals from superdetonative propulsive mode in ethylene-based propellant mixture.

number attained was 8.5 which, as far as the authors know, exceeds the highest operating Mach number of any ramjet discussed in the open literature.

Based on the results of CFD modeling, the combustion mode which drives the projectile in the superdetonative regime is believed to be shock-induced combustion at the lower Mach numbers and oblique detonation waves at the higher Mach numbers.[17,18,48] Regardless of the exact mechanisms, the gas pressure is seen to rise during the combustion process, indicating supersonic heat addition, i.e., a "scram" mode, in the space between the projectile and the tube wall. The experimental variables that affect the superdetonative acceleration performance are currently being investigated.

HYPERSONIC TEST FACILITY APPLICATIONS

Ram accelerator facilities offer two major benefits for hypersonic research. First, the gasdynamic phenomena generated by ram accelerator projectiles are very similar to those expected to occur in scramjet and oblique detonation wave engines, therefore, investigating the different realms of ram accelerator operation will enhance the understanding of hypersonic propulsion phenomena in general. Second, the ability to scale up the bore size and to launch massive objects at hypervelocities, without subjecting them to extreme accelerations, gives the ram accelerator concept the potential to become the launcher of choice for large scale aeroballistic ranges. Some ways to realize these benefits in hypersonic research facilities are discussed below.

In principle, the ram accelerator scales well with size; it has no fundamental upper limit in bore dimension for successful operation. In addition, a scaled-up projectile allows the use of onboard instrumentation, such as pressure transducers, heat transfer gauges, accelerometers, etc. The increase in overall instrumentation density afforded by the larger scale would improve data resolution and enable a greater variety of sensors to be used to better examine the flowfield.[25] High instrument densities result in flowfield measurements that would help develop our understanding of the aerothermodynamic processes occurring in ram accelerators and other

hypersonic propulsive devices, and would be very useful for validating CFD codes that are to be applied to hypersonic vehicles and scramjets.

Additional advantages are associated with adjustments in operating pressure. Experiments have demonstrated that transitions through relatively large pressure differentials can be sustained, which allow projectiles to be ram accelerated up to test speed and then injected into a low pressure test section. The low pressure propellant mixtures result in low accelerations, which would lengthen the test time and improve data resolution from a test section having a fixed instrument density. Low pressure operation would also facilitate use of a transparent section of tube wall for optical and spectroscopic diagnostics of the flow in the ram accelerator. The combination of relatively thin transparent walls and large bore diameters would result in very little optical distortion. Data obtained in such a facility would be directly applicable to current ramjet and scramjet research.

A large-bore ram accelerator tube can be used to launch test models of significant size. Preliminary calculations have been made for large scale ram accelerators based on the experimental results of the UW. These hypervelocity launchers are constrained only by the maximum allowable internal pressure of the accelerator tube and the acceleration limits imposed by the test models. The parameters of the ram accelerator launchers for 30 cm and 60 cm bore facilities, designed to accelerate projectiles having an average density of 1.5 g/cm^3 to a velocity of 6 km/sec, are shown in Table 1. These facilities would be capable of launching projectiles having a total mass of 49 kg and 390 kg, respectively, with a propellant fill pressure of 140 atm. The projectiles, with an external geometry designed for optimal ram acceleration, would act as sabots for the enclosed test models which would be released prior to entering the test section, as discussed below. The estimates for the barrel masses are based on steel walls having the thickness required to keep their internal stress below 4500 atm for a 2250 atm static pressure. This results in a ratio of tube outer to inner diameter of 1.41.

Table 1 Physical parameters for 6 km/sec ram accelerator launchers.

Bore Diameter	30 cm	60 cm
Projectile Mass	49 kg	390 kg
Average Acceleration	6780 *g*	3400 *g*
Barrel Length	270 m	540 m
Barrel Mass	150 tonne	1200 tonne
Fill Pressure	140 atm	140 atm
Peak Pressure	2250 atm	2250 atm

The velocity-distance characteristics corresponding to the launchers described above are shown in Fig. 14. These accelerators are partitioned into four different sections: the initial launcher, thermally choked stages, transdetonative stages, and superdetonative stages. For these scaling examples a conventional gas gun is assumed to bring the projectiles up to an operating speed of 0.7 km/sec. Each of the subsequent phases of ram acceleration involve staging propellant mixtures whose composition is selected to maintain the desired in-tube Mach number and thrust level as the projectile accelerates. Thermally choked propulsion is used up to 3 km/sec, transdetonative up to 4.5 km/sec, and superdetonative up to the final velocity of 6 km/sec. If all of the stages are operated at constant pressure then the partitions between stages could be opened just before launching to allow some mixing at the stage transitions to minimize sudden in-tube Mach number changes and the corresponding acceleration jumps, while also eliminating unnecessary diaphragm impacts. The entrance and exit seals can be burst just before projectile impact to reduce potential projectile and test model damage.

A schematic of an aeroballistic facility using a ram accelerator launcher is shown in Fig. 15. The pre-launcher, ram accelerator section, muzzle vent chamber and sabot stripping

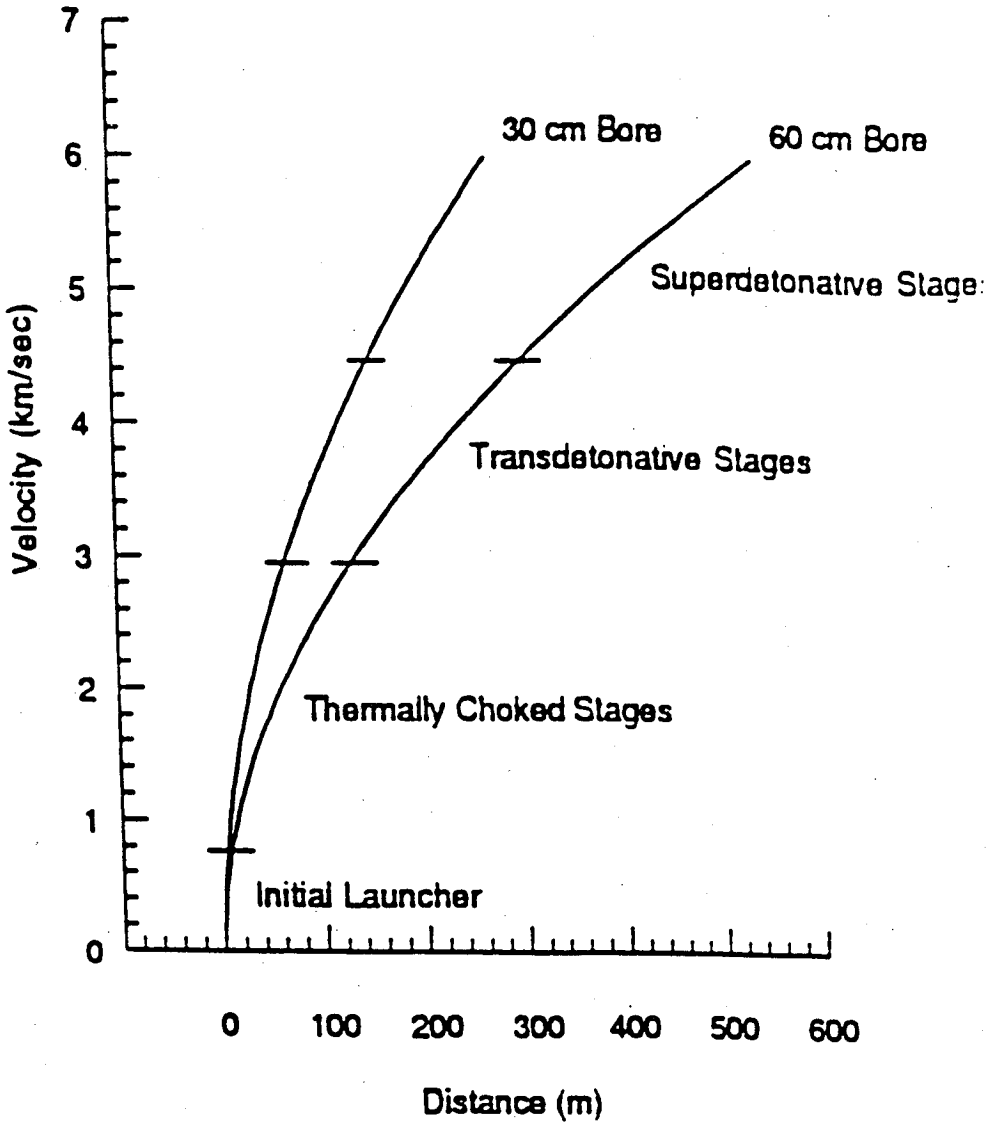

Fig. 14 Velocity-distance profiles of large bore ram accelerators.

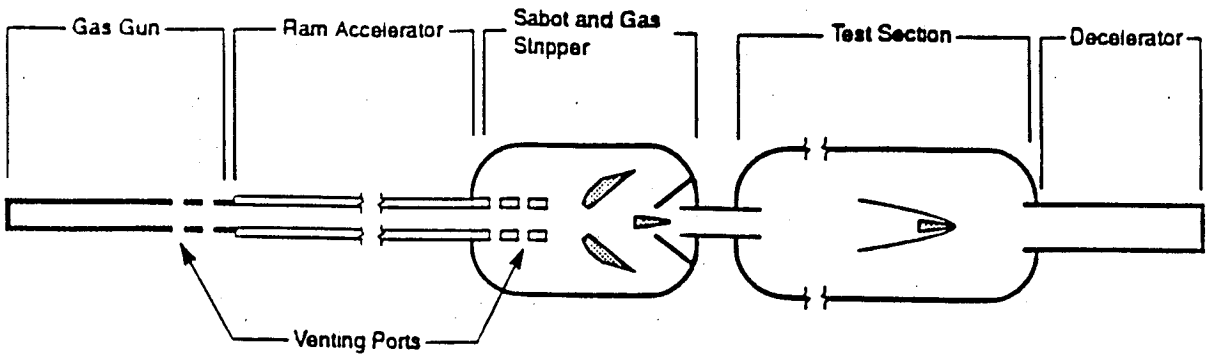

Fig. 15 Schematic of ram accelerator aeroballistic facility.

sections are shown along with a free-flight test section and projectile decelerator. Figure 16 shows an artist's conception of the muzzle vent chamber and sabot stripping sections. An inherent benefit of the ram accelerator launcher is that its muzzle blast is very small compared to that issuing from an equivalent gas gun launch. This is a consequence of the fact that in a ram accelerator the bulk of the burnt propellant gas moves in the rearward direction and is vented at the coupling between the pre-launcher and the ram accelerator. Thus, a short muzzle vent chamber filled with an inert gas would be sufficient to inhibit the remaining muzzle gases from preceding the projectile into the test section.

The sabot stripping section is required to discard the shell of the ram accelerator projectile from the test model. The sabot stripper may use the inert gas within the muzzle vent chamber or the actual test gas. One scenario for this process is shown in Fig. 17. After leaving the ram accelerator section the tip of the nose cone is blown off, which allows the stripping gas to enter the nose cone and pressurize it sufficiently to split it apart along the pre-weakened seams. The high drag profile of the ram accelerator sabot may be sufficient to allow a dense test model to enter the free flight section unencumbered, alternatively, the sabot can be completely fragmented by aerodynamic forces to ensure sufficient separation.

The ballistic coefficient of a large test model is sufficiently high that the flight through low density test gases (simulating upper atmospheres of various planets) would take place at essentially constant speed. The test duration would be governed by the length of the test section. For example, to obtain a 50 msec test duration at 6 km/sec would require a test section 300 m long. Data collected from onboard sensors could be broadcast during transit of the test section or else saved and transmitted before the deceleration phase. The hypersonic test model could be decelerated by conventional means (destructively) after ejecting a data recorder which would be stopped in a less severe manner and interrogated after recovery.[12] It is unlikely that the unconstrained test models can be caught in a soft manner by themselves.

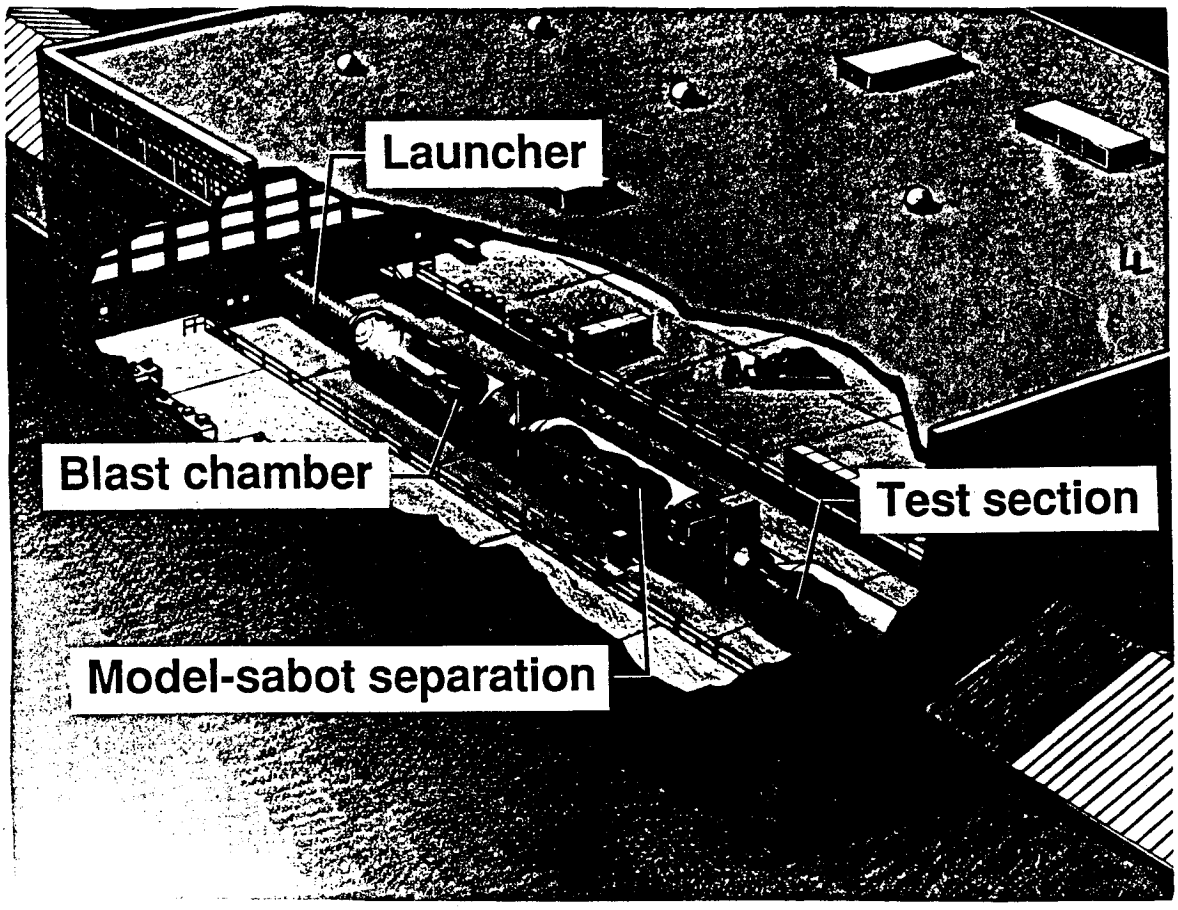

Fig. 16 Artist conception of AHAF research complex using ram accelerator.

(Courtesy of NASA Langley Research Center.)

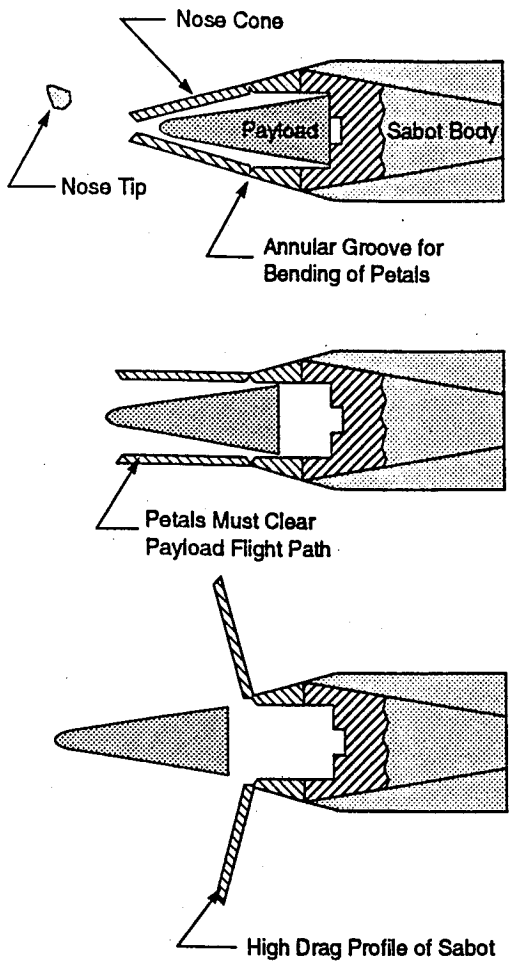

Fig. 17 Ram accelerator sabot separation sequence.

Square Bore Tube

A significant application of the ram accelerator concept to a hypersonic test facility involves using a rectangular bore instead of a circular cross-section.[21,23] With such a modification a two-dimensional, wedge-shaped projectile, sliding along the floor of the square tube, can be propelled by ram accelerator propulsive cycles. The pressure field generated by the shock system would not only produce thrust, but would also press the projectile against the floor, resulting in a stable sliding motion down the tube. Wall friction and ablation can be minimized by coating the projectile surface and the inner tube wall with a layer of Teflon. Rectangular bore ram accelerators scale similarly to round bore designs. For example, a 27-cm square bore ram accelerator has the same cross sectional area as the 30-cm round bore ram accelerator and, consequently, the same length for fixed pressure, mass, and velocity specifications.

A schematic of a rectangular bore ram accelerator hypersonic testing facility is shown in Fig. 18. The projectile is accelerated to the desired test velocity by ram acceleration. Upon exit from the ram accelerator section, the combustible gases are stripped from the projectile in a vent section filled with inert gas, thus preventing the driving gas from expanding into the test section and interfering with the experiment. A two-dimensional carapace sabot could be used to cover the entire length of the test model. Before the sabot-model combination enters the hypersonic test section, the sabot is removed and discarded through an open ceiling in the sabot stripper section.

The model then travels through the test section, which contains the test atmosphere of interest. The test section is on the order of 300 to 500 m in length, which provides test duration times of 50-80 msec for an entrance velocity of 6 km/sec. Having traversed this section, the model enters the decelerator section, which contains an inert gas at a predetermined pressure level. Since the model has a constrained trajectory it is possible to decelerate it in a relatively soft manner by gasdynamic means. Upon entering the decelerator, the model drives a normal shock ahead of it, thus generating sufficient pressure forces to slow the vehicle down. By tapering the ceiling the

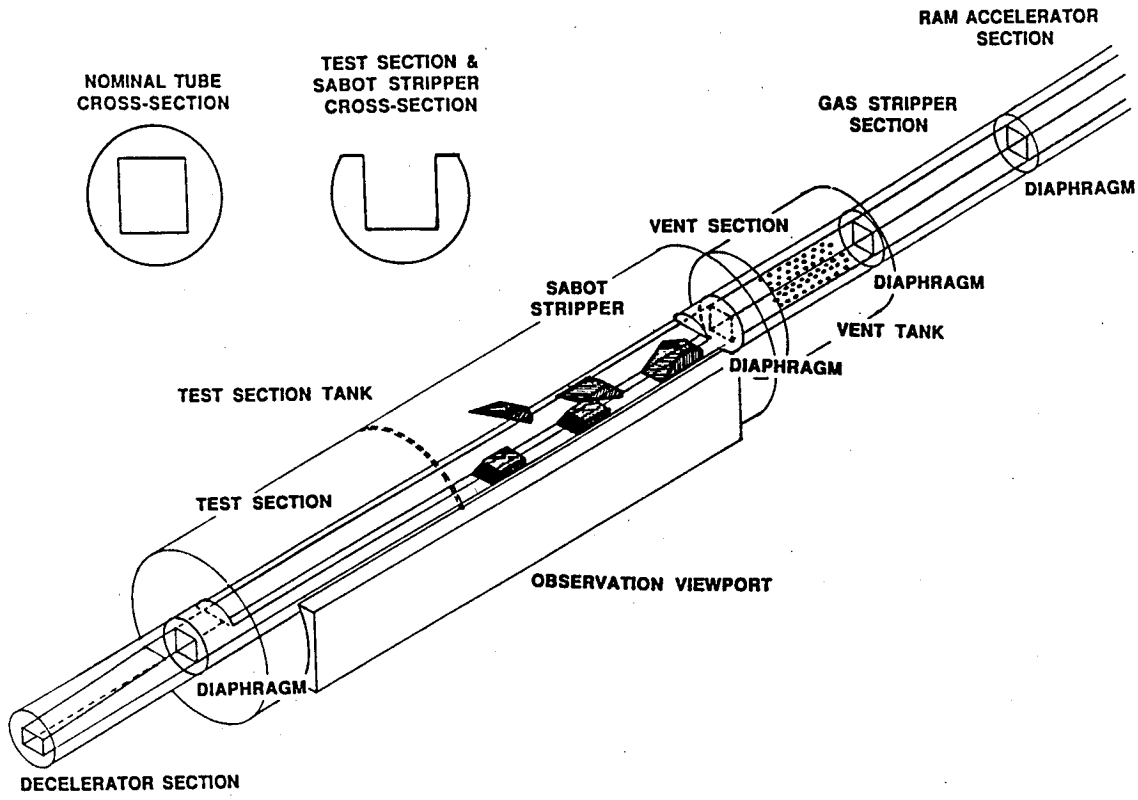

Fig. 18 Rectangular bore ram accelerator hypersonic facility.

deceleration history can be tailored to bring the model to a stop, while keeping the deceleration below destructive levels. This soft catch method preserves any onboard instrumentation.

The primary advantages of a rectangular bore configuration are the ability to use planar windows in the ram accelerator and test section, and the ease of interpreting optical and spectroscopic data from a 2-D rather than a cylindrical parcel of gas. A rectangular bore ram accelerator thus offers an opportunity for direct optical studies of mixing and combustion processes that realistically simulate those in a full-scale hypersonic airbreathing vehicle. For example, the model can be constructed to inject fuel, as shown in Fig. 19, when it reaches the test section atmosphere. Such a configuration would very closely simulate the flow around and through key engine components of the proposed NASP and other hypersonic airbreathing vehicles.

ENGINEERING CONSIDERATIONS

The introduction of new technology, such as the ram accelerator, into the field of hypersonic aerodynamic ground testing naturally gives rise to numerous questions about its engineering feasibility, operational limits, and other critical issues. Several of the most frequently raised issues are discussed below.

Velocity Limits

Ideal inviscid flow computations indicate that the propulsive cycles of the ram accelerator should be capable of accelerating projectiles to velocities of about 10 km/sec.[15] However, recent theoretical work has indicated that the practical velocity limit of the ram accelerator may be closer to 6 to 7 km/sec in hydrogen-diluted propellant mixtures.[49] One of the limiting phenomena appears to be the preignition of the propellant in the stagnation region behind the bow shock at the nose tip of the projectile. At sufficiently high speeds the heating of the propellant at the nose propagates combustion throughout the flow over the nose, resulting in a "doomed propellant fraction," which is burned prior to reaching the throat, resulting in a reduction of thrust. In the UW ram accelerator

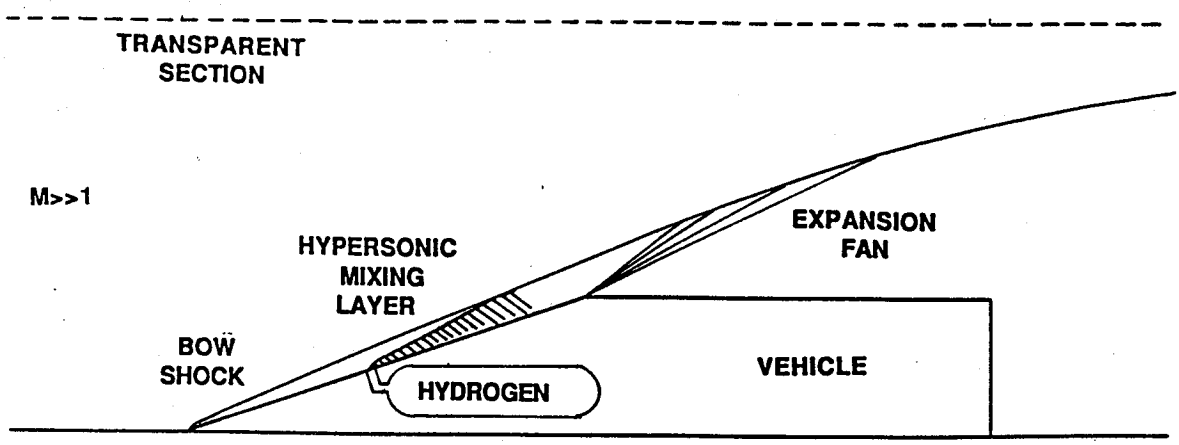

Fig. 19 Hypersonic mixing experiment in 2-D facility.

facility the maximum velocity attained to date is 2.7 km/sec, however, about 3 km/sec should be achievable with relatively minor refinements. This particular limit is governed by factors associated with the length of the laboratory which houses the facility and by the issue of operating safely within a university environment.

Projectile Geometry and Fin Wear

The basic projectile geometry that is currently used in experiments at the UW has not changed much since the beginning of our experimental program. Indeed, researchers at ISL in France[39] and at BRL in this country[33] are also using identical, scaled-up projectile geometries. Various configurations have been investigated at the UW from time to time. Presently, the most promising change to the conventional body geometry appears to be the use of five fins rather than four, for both structural and aerothermodynamic reasons.[25,26]

It is clear that the geometric features which provide potential for high speed reliability and propulsive mode optimization need to be systematically quantified. Examples of geometric parameters that should be investigated include the throat-to-tube and base-to-tube area ratios, projectile length, nose cone angle and contour, body taper angle, number of fins, fin thickness profile, and fin leading edge shape and rake angle.

Fin damage can occur at any velocity, due to improper operational procedures, inadequate fin design, and unsuitable material selection. The use of magnesium and aluminum alloys to date has been an expedient, motivated by cost considerations. These materials (especially the 7075-T6 aluminum alloy) offer high strength-to-weight ratio at low cost, have performed satisfactorily at velocities up to 2.7 km/sec and are expected to be usable up to 3 km/sec. It is clear, however, that these materials are far from optimum for higher velocity applications, especially at large scale.

The possibilities of composite materials for ultrahigh velocity applications will need to be explored. A composite projectile can mean either of two options: 1) the use of advanced composite materials, such as carbon-carbon or metal matrix composites for the entire projectile;

2) the use of different materials for the various parts of the projectile, e.g., copper-clad titanium or composite nose cone, aluminum body, and composite fins; or, perhaps, aluminum fins with composite bearing surfaces.

Another approach to reducing fin wear is to actively enhance the lubricating effects of the gas film which forms in the narrow gap between the fins and the barrel wall. This could be accomplished, for example, by appropriately shaping the fin contact surfaces to channel the propellant gas into the interface gaps. (It should be remembered that the fins are designed only to keep the projectile body off the wall and do not necessarily have to be in intimate contact with the wall.) Alternatively, lubricants can be injected from the projectile into the interface gap to reduce the fin heating.

Barrel Design

Barrel design for a large-scale facility is not expected to present unusual problems. The UW ram accelerator barrel is fabricated from 4150 steel alloy. Barrel heating and erosion have not been significant. The first barrel was used for 647 shots before being replaced for reasons having to do with instrument port size and spacing, original bore diameter profile, and other factors unrelated to barrel wear. Although many shots up to 2.5 km/sec were performed in the old barrel sections, they suffered very little erosion. The current barrel has supported more than 300 shots, many at the high end of the velocity range, i.e., 2.2 to 2.7 km/sec. Again, barrel wear has not been significant, even in the highest speed sections, and it is expected that this barrel will continue to be used for many more shots.

The issue of large scale barrels, specifically for application to ram accelerator mass launchers, has received preliminary attention.[50,51] Both conventional steel alloys and composite materials could be used. The aspect of design that differs from that of conventional gun-type launchers is that the ram accelerator propulsive modes generate a traveling pressure pulse rather

than a distributed pressure load. Thus, the dynamics of the acceleration process will have to be considered when optimizing the design of the barrel.

Another aspect of barrel design is whether to center the projectile by means of fins on the projectile or rails on the barrel. For small laboratory-scale ram accelerators the projectile fin approach is simpler and more flexible, allowing the experimenter to vary the projectile geometry in a straightforward manner. To date all experimental ram accelerators have used this approach. In a large-scale ram accelerator centering rails can be more easily implemented and offer significant mass savings through the elimination of the fins on the projectile. Small-scale experiments with a railed tube are about to be undertaken at ISL.[40]

In-tube Aerodynamic Heating

In-tube aerodynamic heating is a significant concern for a projectile traveling at 7 km/sec or more through a pressurized gas environment such as found in a ram accelerator. Recently, computations have been performed at NASA Ames Research Center on the effects of heat transfer to a large scale projectile (76 cm dia x 7.5 m long, with a 7° nose cone angle) being ram accelerated to velocities of 7 and 10 km/sec by means of an oblique detonation propulsive mode in a propellant mixture consisting of $8H_2+O_2$.[52] The heat transfer at the nose tip and on the body in the region of maximum pressure was investigated, and the ablated mass loss and dimensional change which would occur with a carbon composite projectile material were calculated. The results at 7 km/sec indicate that the mass loss and dimensional change at the nose are very small (~$2x10^{-3}$% and $5x10^{-3}$%, respectively). The ablation on the projectile body at the maximum pressure region is greater, resulting in a 2.5% reduction in radius and a 5% mass loss. (At 10 km/sec the heating is severe enough to destroy the projectile, however, this may be circumvented by operating the projectile within an inner core of low molecular weight gas (H_2 or He) at velocities above 7 km/sec.[15]) Thus, at velocities up to 7 km/sec in-bore aerodynamic heating does not appear to present insurmountable problems. The use of appropriate carbon composite ablative coatings will be sufficient to assure projectile survival.

Diaphragms and Closures

The pressurized propellant gases in the existing experimental ram accelerator facilities have been contained in the accelerator tubes by means of Mylar or PVC diaphragms up to 25 mm thick. No projectile damage has been observed to result from the puncturing of diaphragms by projectiles moving at velocities up to 2.7 km/sec. As the ram accelerator is scaled up, so must the thickness of the diaphragms increase. At scales of 30 to 60 cm bore the use of passive diaphragms may not be practical or feasible, therefore some other type of closure may have to be used. Various possibilities exist, such as fast-acting mechanical closures similar to ball valves or gate valves, or thin metallic diaphragms equipped with shaped charges to effect rapid opening before projectile impact.

Initial Launcher

In order for the ram acceleration process to begin, the projectile must be moving above Mach 2.5 with respect to the propellant gas, as noted earlier. To date this requirement has been met by means of a light gas gun launcher (UW and APRI) or a powder gun launcher (ISL and BRL). Scaling a gun up to a large scale while maintaining soft launch capabilities is a challenging task, but may not be necessary. The authors have devised a means of initiating the ram acceleration process with the projectile at rest.[27] This entails configuring the initial section of ram accelerator as a backward pointing expansion tube. To start the process the first diaphragm or mechanical closure is suddenly opened, releasing propellant gas in a free expansion towards the stationary projectile (which is backed by an appropriate obturator). The gas velocity meeting the projectile is supersonic and the flow interaction with the obturator ignites the gas at the projectile base.[29] Thrust is generated and the projectile begins to accelerate until it overtakes the forward moving expansion front in the ram accelerator.

This so-called "zero velocity start" technique has not yet been experimentally demonstrated but plans have been made to do so shortly. It offers the possibility of true soft launch via a ram

accelerator process from beginning to end, and the consequent elimination of the problems associated with a gun-type pre-launcher.

CONCLUSION

The development of ram accelerator technology at the University of Washington and elsewhere has given rise to the possibility of "soft" launching relatively large-scale test models and full-sized components of hypersonic vehicles at realistic velocities in a large-scale aeroballistic range facility. Ram accelerator operation has been demonstrated at 38 mm bore at the University of Washington, and at 90 mm and 120 mm bores elsewhere, supporting the proposition that this launcher concept can be scaled up to very large bore diameters, of the order of 30 - 60 cm.

Three velocity regimes, centered about the C-J detonation velocity, have been identified that exhibit different acceleration characteristics, indicating the existence of several different propulsive cycles. Low supersonic Mach number (Mach 3 to 4) performance is predicted very well by a one-dimensional Hugoniot model for the case of thermal choking behind the projectile. Transdetonative performance is characterized by the forward motion of the combustion process up onto the projectile body and the existence of regions of mixed supersonic and subsonic combustion. Single-stage experiments have driven projectiles up to Mach numbers at which a reflected oblique shock wave can induce the combustion process to occur totally on the projectile body, which further propels the projectiles to hypersonic speeds. Superdetonative acceleration has been demonstrated in the Mach number range of 7 to 8.5 in ethylene-based propellant mixtures. Data collected from the tube wall and projectile during the acceleration process itself are very useful for understanding the aerothermodynamics of hypersonic flow in general, and for providing important CFD validation benchmarks.

Although projectile acceleration at velocities above 3 km/sec has yet to be experimentally demonstrated, the technical and material problems expected at hypervelocities in high pressure, gaseous propellant mixtures appear to be surmountable with relatively modest research efforts.

REFERENCES - CHAPTER I

1. William, R.M., "National Aerospace Plane: Technology for America's Future," Aerospace America, Vol. 24, Nov. 1986, pp. 18-24.

2. Walberg, G.D., "A Survey of Aeroassisted Orbital Transfer," J. Spacecraft & Rockets, Vol. 22, 1985, pp. 3-18.

3. Anderson, J.D., Hypersonic and High Temperature Gasdynamics, McGraw-Hill Book Co., New York, 1989.

4. Anderson, J.D., "A Survey of Modern Research in Hypersonic Aerodynamics," AIAA Paper No. 84-1578, June 1984.

5. Strawa, A.W., Chapman, G.T., Canning, T.N., and Arnold, J.O., "Ballistic Range and Aerothermodynamic Testing," J. Aircraft, Vol. 28, 1991, pp. 443-449.

6. Lukasiewitz, J., Experimental Methods of Hypersonics, Marcel Dekker, Inc., New York, 1973.

7. Stalker, R.J., "Recent Developments with Free Piston Drivers," Current Topics in Shock Waves, Kim, Y.W., ed., AIP Conference Proceedings 208, American Institute of Physics, New York, 1990, pp. 96-105.

8. Miller, C.G., "Operational Experience in the Langley Expansion Tube with Various Test Gases," NASA TM 78637, NASA Langley Research Center, Hampton, VA, December 1977.

9. Canning, T.N., Seiff, A., and James, C.S., eds., Ballistic Range Technology, North Atlantic Treaty Organization Advisory Group for Aerospace Research and Development, AGARD-ograph No. 138, August 1970.

10. Squire, W., Hertzberg, A., and Smith, W.E., "Real Gas Effects in a Hypersonic Shock Tunnel," Report No. AD-789-A-1, Cornell Aeronautical Laboratory, Buffalo, NY, 1955.

11. Glick, H.S., Squire, W., and Hertzberg, A., "A New Shock Tube Technique for the Study of High Temperature Gas Phase Reactions," Proceedings of the Fifth Symposium (International) on Combustion, Pittsburgh, PA, Aug. 30 - Sept. 3, 1955, Reinhold Publishing Corp., New York, pp. 393-402.

12. Witcofski, R.D., Scallion, W.I., Carter, D.J., and Courter, R.W., "An Advanced Hypervelocity Aerophysics Facility: A Ground-Based Flight Test Range," AIAA Paper 91-0296, January 1991.

13. Barber, J., "Hypervelocity Railguns for Aeroballistic Testing," AIAA Paper 92-3948, July 1992.

14. Hertzberg, A., Bruckner, A.P., and Bogdanoff, D.W., "Ram Accelerator: A New Chemical Method for Accelerating Projectiles to Ultrahigh Velocities," AIAA Journal, Vol. 26, 1988, pp. 195-203.

15. Knowlen, C., Bogdanoff, D.W., Bruckner, A.P., and Hertzberg, A., "Performance Capabilities of the Ram Accelerator," AIAA Paper 87-2152, June 1987.

16. Bruckner, A.P., Knowlen, C., Hertzberg, A., and Bogdanoff, D.W., "Operational Characteristics of the Thermally Choked Ram Accelerator," J. Propulsion and Power, Vol. 7, 1991, pp. 828-836.

17. Yungster, S., Eberhardt, S., and Bruckner, A.P. "Numerical Simulation of Hypervelocity Projectiles in Detonable Gases," AIAA J., Vol. 29, February 1991, pp. 187-199.

18. Yungster, S. and Bruckner, A.P., "Computational Studies of a Superdetonative Ram Accelerator Mode," J. Propulsion and Power, Vol. 8, 1992, pp. 457-463.

19. Kull, A.E., Burnham, E.A., Knowlen, C., Bruckner, A.P., and Hertzberg, A., "Experimental Studies of Superdetonative Ram Accelerator Modes," AIAA Paper 89-2632, July 1989.

20. Burnham, E.A., Kull, A.E., Knowlen, C., Bruckner, A.P. and Hertzberg, A., "Operation of the Ram Accelerator in the Transdetonative Velocity Regime," AIAA Paper 90-1985, July 1990.

21. Hertzberg, A., Bruckner, A.P., and Knowlen, C., "The Ram Accelerator as a Hypersonic Test Facility," AIAA 16th Aerodynamic Ground Testing Conference, Seattle, WA, June 18-20, 1990. (Post-deadline paper).

22. Hertzberg, A., Bruckner, A.P., and Knowlen, C., "Experimental Investigation of Ram Accelerator Propulsion Modes," Shock Waves, Vol. 1, 1991, pp. 17-25.

23. Bruckner, A.P., Chew, G., Auzias de Turenne, J., and Dunmire, B., "Investigation of Hypersonic Ramjet Propulsion Cycles Using a Ram Accelerator Test Facility," Paper No. IAF 91-275, 42nd Congress of the International Astronautical Federation, Montreal, Canada, October 5-11, 1991.

24. Knowlen, C., Bruckner, A.P., and Hertzberg, A., "Internal Ballistics of the Ram Accelerator," 13th International Symposium on Ballistics, Stockholm Sweden, June 1-3, 1992.

25. Hinkey, J., Burnham, E., and Bruckner, A.P., "High Spatial Resolution Measurements of Ram Accelerator Gas Dynamic Phenomena," AIAA Paper, 92-3244, July 1992.

26. Auzias de Turenne, J., Chew, G., and Bruckner, A.P., "Recent Progress in Ram Accelerator Technology," AIAA Paper 92-3782, July 1992.

27. Hertzberg, A., Bruckner, A.P., Knowlen, C., and McFall, K., "A Method and Apparatus for Zero-Velocity Start of Ram Accelerator Projectiles," U.S. Patent No. 5,097,743, March 24, 1992

28. Knowlen, C., Li, J.G., Hinkey, J., and Dunmire, B., "University of Washington Ram Accelerator Facility," 42nd Meeting of the Aeroballistic Range Association, Adelaide, Australia, October 22-25, 1991.

29. Bruckner, A.P., Burnham, E.A., Knowlen, C., Hertzberg, A., and Bogdanoff, D.W., "Initiation of Combustion in the Thermally Choked Ram Accelerator," Paper No. F14, Proceedings of the 18th International Symposium on Shock Waves, Sendai, Japan, July 21-26, 1991, in press.

30. Henderson, B.W., "Ram Accelerator Demonstrates Potential for Hypervelocity Research, Light Launch," Aviation Week & Space Technology, Vol. 135, Sept. 30, 1991, pp. 50-51.

31. Kruczynski, D.L., "Analysis of Ram Accelerator for High Velocity Applications," AIAA Paper No. AIAA-91-2488, June 1991.

32. Nusca, M.J., "Numerical Simulation of Reacting Flow in a Thermally Choked Ram Accelerator Projectile Launch System," AIAA Paper 91-2490, June 1991.

33. Kruczynski, D.L. and Nusca, M.J., "Experimental and Computational Investigation of Scaling Phenomena in a Large Caliber Ram Accelerator," AIAA Paper 92-3245, July 1992.

34. Sinha, N., Dash, S., Drabczuk, R., Rolader, G., Progress Toward the Development of Transient Ram Accelerator Simulation and Overview of U.S. Air Force Armament Directorate Research Program," AIAA Paper 92-3248, July 1992.

35. Yungster, S., "Navier Stokes Simulation of the Supersonic Combustion Flowfield in a Ram Accelerator," AIAA Paper No. 91-1916, June 1991.

36. Li, C., Kailasanath, K., and Oran, E.S., "Oblique Detonations in Ram Accelerators," 28th JANNAF Combustion Subcommittee Meeting, Brooks AFB, TX, Oct. 28 - Nov. 1, 1991.

37. Soetrisno, M., Imlay, S.T., and Roberts, D., "Numerical Simulation of the Transdetonative Ram Accelerator Combusting Flowfield on a Parallel Computer," AIAA Paper No. 92-3249, July 1992.

38. Humphreys, J.W. and Sobota, T.H., "Beyond Rockets: the Scramaccelerator," Aerospace America, Vol. 29, June 1991, pp.18-21.

39. Giraud, M., Legendre, J.F., Simon, G., and Catoire, L., "Ram Accelerator in 90 mm Caliber: First Results Concerning the Scale Effect in Thermally Choked Propulsion Mode," 13th International Symposium on Ballistics, Stockholm, Sweden, June 1-3, 1992.

40. Smeets, G. and Srulijes, J., Institut Franco-Allemand de Recherches, St. Louis, France, Private Communication, June 1992.

41. Knowlen, C. and Bruckner, A.P., "A Hugoniot Analysis of the Ram Accelerator," Paper No. F13, Proceedings of the 18th International Symposium on Shock Waves, Sendai, Japan, July 21-26, 1991, in press.

42. Ostrander, M.J., Hyde, M.F., Young, R.D., and Kissinger, R.D., "Standing Oblique Detonation Wave Engine Performance," AIAA Paper 87-2002, June 1987.

43. Pratt, D.T., Humphrey, J.W., and Glenn, D.E., "Morphology of a Standing Oblique Detonation Wave," J. Propulsion and Power, Vol. 7, 1991, pp. 837-845.

44. Bogdanoff, D.W., Knowlen, C., Murakami, D., and Stonich, I.,"A Magnetic Detector for Projectiles in Tubes," AIAA Journal, Vol.28, 1990, pp.1942-1944.

45. Dunmire, B., "An Experimental and Theoretical Investigation of Single Stage Ram Accelerator Performance with Emphasis Towards Projectile Material Effects," M.S.A.A.

Thesis, Department of Aeronautics and Astronautics, University of Washington, Seattle, WA, September 1991.

46. Auzias de Turenne, J., "An Analysis of Ram Accelerator Projectile Materials," AIAA Paper No. 92-0262, AIAA 30th Aerospace Sciences Meeting and Exhibit, Reno, NV, January 6-9, 1992.

47. Yungster, S. and Bruckner, A.P., "A Numerical Study of the Ram Accelerator in the Superdetonative Velocity Range," AIAA Paper No. 89-2677, July 1989.

48. Nusca, M.J., "Numerical Simulation of Reacting Flow in a Thermally Choked Ram Accelerator," 27th JANNAF Combustion Subcommittee Meeting, Cheyenne, Wyoming, November 5-9, 1990.

49. Ghorbanian, K., Pratt, D.T., and Humphrey, J.W., "Supersonic Flow of Reactive Gases Over Sphere-Cone Bodies," AIAA Paper 92-0091, January 1992.

50. Bruckner, A.P. and Hertzberg, A., "Ram Accelerator Direct Launch System for Space Cargo," Paper No. IAF-87-211, 38th Congress of the International Astronautical Federation, Brighton, England, October 10-17, 1987.

51. Kaloupis, P. and Bruckner, A.P., "The Ram Accelerator: A Chemically Driven Mass Launcher," AIAA Paper 88-2968, July 1988.

52. Bogdanoff, D.W., "Ram Accelerator Direct Space Launch System: New Concepts," J. Propulsion and Power, Vol. 8, 1992, pp. 481-490.

II. FLOWING GAS RADIATION RECEIVER

INTRODUCTION

The flowing gas radiation receiver (FGRR) is a novel concept for using solar energy to heat a working fluid for space power or propulsion. It was initially studied at the University of Washington under NASA sponsorship in the 1979-1983 time period, to determine its capabilities and advantages for space applications. Under the present NASA grant, a key issue relating to its effectiveness - trapping of reradiation - was studied experimentally. This study demonstrated that radiation trapping does indeed enhance the performance of the FGRR, allowing generation of higher temperatures than are possible using a simple blackbody receiver. This chapter reviews the FGRR concept in a background section, then presents the results of the studies on radiation trapping in an experiment section.

BACKGROUND

The basic idea behind the flowing gas radiation receiver is presented in Fig. 20. Focused solar radiation is directed into the entrance of an absorption channel which also conveys a working gas in the same direction as the radiation propagation axis. The fluid is seeded with a small quantity of gas which is an efficient absorber of solar radiation. As the gas traverses the channel, it absorbs the radiation, increasing the temperature to a peak value at the channel outlet. The heated gas can then be used as a working fluid in a power cycle or for thrust as a propellant.

The chief advantage of this approach for using solar energy is the use of direct volumetric heating of a gas, without need for heat transfer through a solid surface. The core of the gas flow can reach temperatures far beyond peak temperatures of heat transfer materials, leading to improved efficiency in power cycles or enhanced specific impulse for propulsion. The walls of the absorption chamber can be kept at relatively low temperatures. As shown in Fig. 20, the walls can actually be cooled as they transfer heat to the fluid fed to the chamber, which serves as a regenerative heat exchanger.

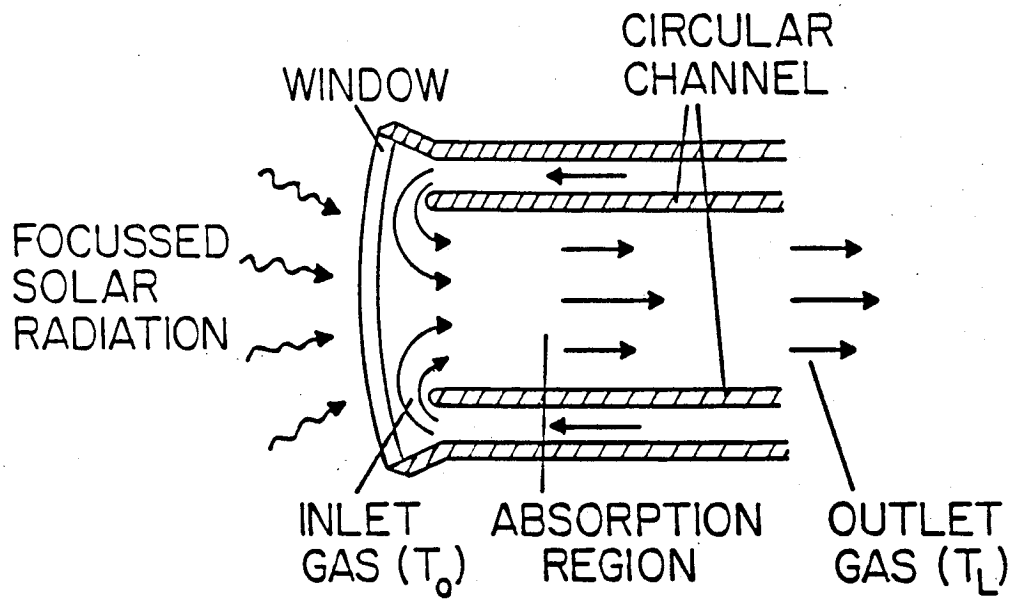

Fig. 20 Illustration of the flowing gas radiation receiver concept.

A key feature of the FGRR is its inherent ability to trap reradiation - that is, radiation by the heated gas is at least partially absorbed before escaping the entrance window. This phenomenon arises by virtue of the collinearity of radiation and gas propagation axes. The gas nearer the window is relatively cool because only a small fraction of the incoming radiation has been absorbed, and it radiates to a lesser extent than the hotter gas downstream. The more intense radiation by downstream gas is absorbed by this cooler gas nearer the window and is not lost out the window. This feature allows the generation of higher temperatures than are possible using a blackbody receiver exposed to the same flux, although the FGRR makes use of all the available solar radiation (provided that the seedant absorbs effectively over most of the solar spectrum).

The radiation receiver was initially described in Ref. 1, which considered the use of potassium vapor as a working fluid for a high-temperature Rankine power cycle for space. Potassium was shown to exhibit a suitable absorption spectrum at high temperatures to provide efficient absorption over virtually the entire solar spectrum, with practical absorption lengths on the order of 1 meter. Using a simple 1-D model, it was predicted that temperatures approaching 4000 K might be achieved. A wave-energy exchanger[2] was employed to enable use of such high temperatures for efficient power production, and thermal efficiencies as high as 75% were predicted for the binary cycle examined.

A theoretical study of radiation transfer in the FGRR was carried out and presented in Ref. 3. This study focused on examining how radiation trapping enhances the efficiency of this receiver in comparison to solid-surface receivers (such as a blackbody cavity). A 1-D model of the receiver was used, on the assumption that the walls of the absorption channel were highly reflecting, and that the convective transport of energy to the walls was small. Gases having both gray and non-gray absorption spectra were examined, the latter modeled by a "picket-fence" spectrum, with discrete bands having constant absorption coefficient. Local thermal equilibrium was assumed, since at the high operating temperatures used, the transfer of electronic energy to vibration, translation, and rotation is quite fast. Even for the simple model used, the radiation

transfer is governed by an integro-differential equation, which required an iterative numerical solution.

Figure 21 shows a key result of this study. The receiver efficiency (fraction of incident solar power retained in the gas) is plotted against fluid outlet temperature for gases with gray spectra, and for two non-gray spectra, and compared with the efficiency of a blackbody receiver. The non-dimensional outlet temperature is scaled by $T_e=(I/\sigma)^{1/4}$, where I is the intensity of the incident radiation and σ is the Stephan-Boltzmann constant. T_e is the temperature an insulated blackbody would reach if exposed to radiation intensity I. For example, with an intensity 1/6 that of the sun's surface (a value achievable using a space-based solar concentrator), T_e=3850K. For all spectra the FGRR efficiency exceeds that of a blackbody over a wide temperature range. The non-gray spectra had two bands of absorption, parameterized by the relative absorption in each band, and the wavelength separating the bands. "A" spectra, with stronger absorption at long wavelengths exhibited efficiencies significantly higher than gray gases, while "B" spectra, having stronger absorption at short wavelengths, were less efficient than gray gases. The best case found in this study exhibited a receiver efficiency of 80% at a relative gas outlet temperature of 0.9 (absolute temperature of 3080K for T_e=3850K), whereas a blackbody receiver efficiency is only 30% owing to the large reradiation losses at this temperature.

An experiment was conducted at the University to measure enthalpy gain in potassium vapor heated with radiation from a solar simulator.[4,5] This experiment indeed demonstrated that the FGRR is capable of heating an absorbing gas to high temperatures, but the relatively small scale of the absorption chamber resulted in large convective heat transfer to the channel walls, so that the effects of radiation trapping could not be measured. A study of application of the radiation heater to space propulsion was also carried out in the same time period.[6] This study demonstrated that the FGRR is very competitive for orbit transfer applications. An ISP of about 1000 sec was computed, significantly above that for chemical propulsion, at thrust levels of 400-2000N, much higher than those reached by electric propulsion. In 1988-89 a solar-powered FGRR for propulsion was examined and compared with laser-powered and MPD thrusters as

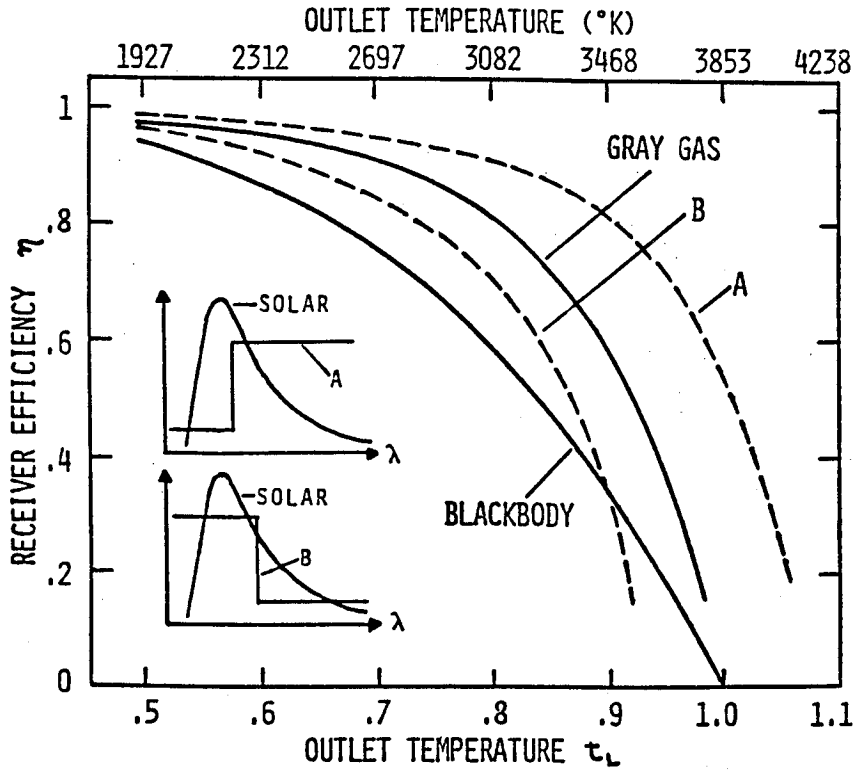

Fig. 21 Theoretical values of radiation heater efficiency vs gas outlet temperature, for a blackbody and for the FGRR using a gray gas and 2 nongray gases. FGRR results are for a 1-D radiation transfer model. [Ref. 2]

improved alternatives for chemical thrusters for Mars missions, under a NASA/USRA sponsored design project at the University of Washington.[7] The FGRR thruster was shown to have the highest payload fraction (37%) and lowest initial mass of the three advanced thrusters, resulting in a greatly reduced trip time (281 days vs. 2.4 years for a chemical thruster). This advantage resulted from the combination of high ISP and high thrust attainable with the FGRR.

More recently McFall and Mattick[8,9,10] and Thynell and Merkle[11] have investigated the interaction of flow with radiation transfer in the FGRR in more realistic 2-D models. These studies predict somewhat lower peak temperatures and efficiencies than the earlier 1-D models, but still show that the FGRR exceeds the performance of blackbody receivers. Again, a primary reason for the high performance is radiation trapping. For this reason, an experimental program was carried out under this grant to demonstrate that radiation trapping results in higher temperatures than are attainable without trapping. This program is discussed in the following section.

MEASUREMENT OF RADIATION TRAPPING IN THE FGRR

Because of the central importance of radiation trapping for achieving high temperatures and high efficiencies in the flowing gas radiation receiver, an experimental demonstration of this trapping was carried out, along with a theoretical analysis of heat transfer in the experimental FGRR to interpret the results. To avoid the complications of using an alkali vapor for radiation absorption, as was done in a previous experimental program on the FGRR[4,5], it was decided to use less reactive species and monochromatic radiation from a laser, rather than broadband radiation simulating the solar spectrum. Although the absorption process is markedly different from that of a solar-powered radiation heater, the radiation trapping is quite similar, and the results of this experiment serve to demonstrate the advantage of trapping. Moreover, the FGRR can in fact be utilized to absorb *laser*, rather than solar, radiation for space power and propulsion,

and this experiment is directly applicable to these purposes. This program was carried out as a Master's thesis at the University, and full details can be found in Ref. 12.

a) Experiment design

The radiation source for the experiment was a nominally 20-Watt CO_2 CW laser available in our laboratory, and the characteristics of the laser (power and wavelength) established the scale and working gas for the experiment. The laser operated on the 10μm P(20) line. Sulfur hexafluoride (SF_6) was chosen as a "seedant" (equivalent to an alkali vapor in a solar-heated receiver) because of its strong and well-characterized absorption of CO_2 laser radiation, and previous use for heating gases with CO_2 lasers.[13,14,15]

To isolate the effects of radiation energy transfer from convection heat transfer to the walls of the flow channel, both infrared-active and infrared-inactive gases were used as "working gases". Carbon dioxide was used as an IR-active gas, wherein radiation transport (including trapping) plays an essential role in establishing the temperature profile in the flow. At the temperatures used (up to about 700K) CO_2 gas absorbs the CO_2 laser radiation only very weakly in comparison to the SF_6 seedant, so the deposition of energy in the flow could be made the same in CO_2 as in IR-inactive gases. Argon and nitrogen were used as IR-inactive gases, wherein convection alone determines the energy transfer in the flow. In both cases the mole fraction of SF_6 was very low ($\leq$ 1.5 mole percent), so although the SF_6 absorption at the laser wavelength was responsible for heating the gas, the integrated absorption coefficient (and emissive power) was so small as to have negligible effect on energy transport in the flow.

The experimental configuration is shown in Fig. 22. The laser beam is directed into a vertically aligned absorption chamber to eliminate azimuthal asymmetries from buoyancy effects. The radiation enters the chamber through a NaCl window, heating the SF_6-seeded gas, and the gas temperature is measured at several axial and radial stations throughout the chamber using a type K thermocouple inserted from the rear of the channel through a high-temperature O-ring seal. The thermocouple was covered with a gold-foil to eliminate radiation transfer from effecting

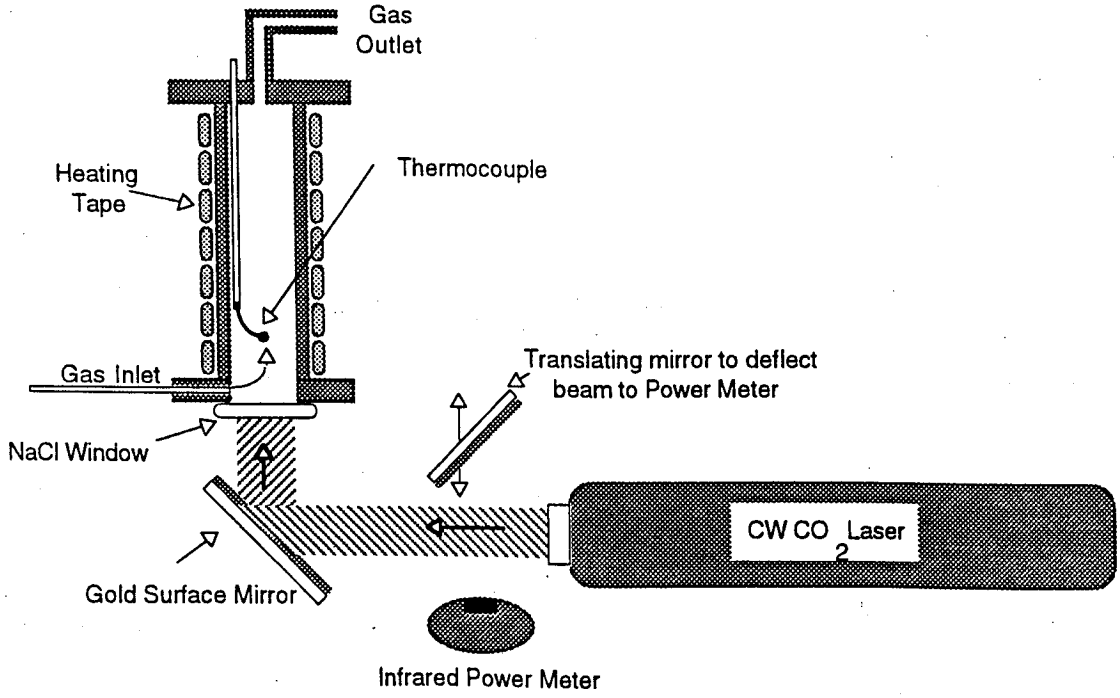

Fig. 22 Experimental setup for measuring radiation trapping in the FGRR.

temperature measurement. The laser power was periodically monitored by an IR power meter, and the fraction of energy entering the chamber via the beam-directing mirror and window was measured to be 0.887. For most runs the laser peak power was 23 W, with a slow oscillation of about 5%. All the data was taken at the peak of this oscillation. The beam diameter was 15 mm.

A schematic of the absorption chamber is shown in Fig. 23. The interior flow channel was constructed of a 1.73-cm ID, 15-cm long stainless steel tube turned down to a thickness of 0.5 mm to minimize axial heat transfer. To facilitate analysis, the chamber was designed to keep the walls adiabatic as far as possible, so that the wall temperature would approximate the average gas temperature at a given axial location. To this purpose, the inner channel was plated with Ni (emissivity of $\approx$ 6% at 600K) to minimize absorption of radiation, and was surrounded by a vacuum jacket with Ni and Cu radiation shields interposed between the channel and the outer wall. In addition, the outer wall and end flanges were actively heated using heat tapes, with the upstream flange kept at 533$\pm$2K (limited by temperature constraints on the NaCl window), and the downstream flange kept at 673$\pm$1K. The temperature of the inner chamber was measured at 2.25 cm, 7.5 cm, and 14 cm from the back face of the window, and the temperature profile was estimated by the polynomial fits shown in Fig. 24. This wall temperature profile was used in the theoretical model of the experimental FGRR in predicting gas temperature profiles.

To achieve an axisymmetric flow, the gas was introduced through 6 equally-spaced inlets near the front window, with the flow helping to moderate the window temperature. Secondary inlets were provided downstream to allow introduction of absorbing gas away from the window to minimize window heating. However, it was decided not to utilize these ports, because of the difficulty of modeling the more complex flow. The gas flow was controlled by fine metering valves, and measured using high accuracy rotameters. The estimated accuracy is 5%. Flow speeds in the absorption chamber ranged from 1 cm/sec to 15 cm/sec, and the fraction of SF_6 ranged from 0.01% to 1.5% by mole. The flow exited the chamber through a small port in the back flange, this flange being Ni-plated, like the inner channel, to minimize absorption or emission of radiation.

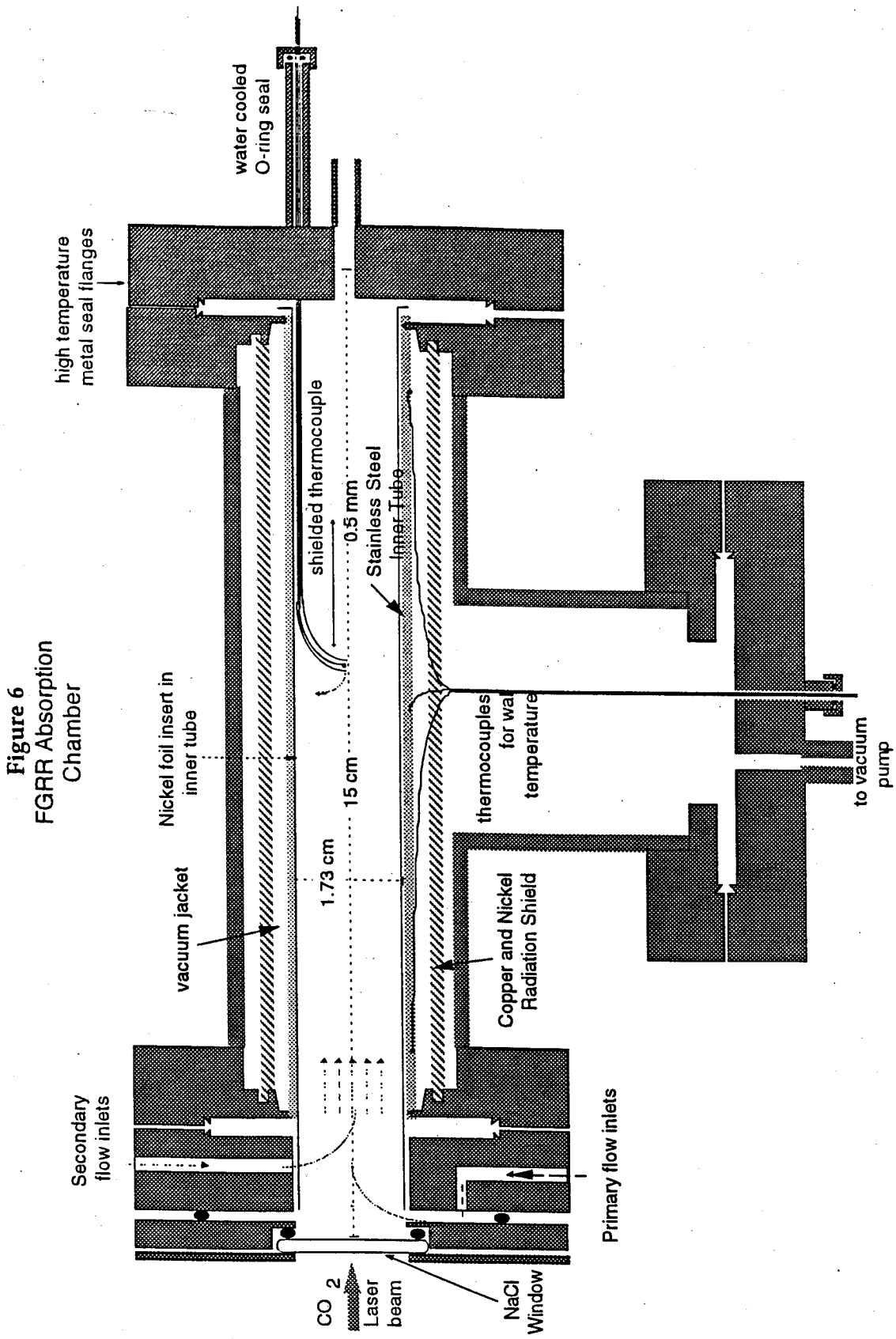

Figure 6
FGRR Absorption
Chamber

Fig. 23 Schematic of FGRR absorption chamber.

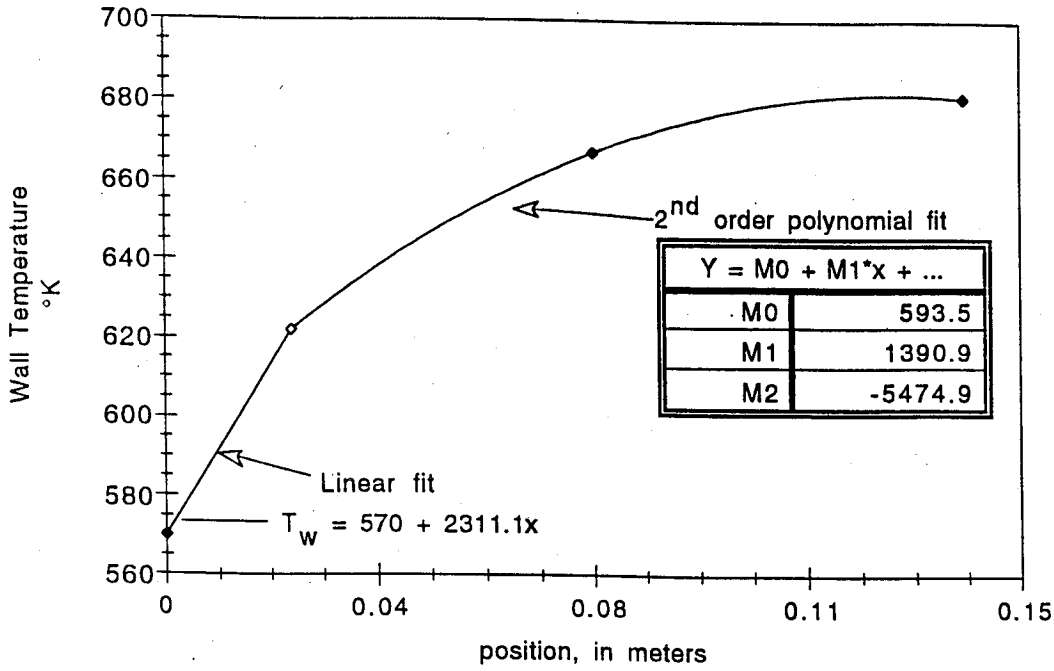

Fig. 24 Measured FGRR wall temperature, and polynomial fitting parameters.

b) Analytical model

A model of heat transfer in the experimental FGRR chamber was developed to allow determination of radiation trapping effects from the experimental temperature profile. This model incorporated the 1-D radiation transfer formalism used by Mattick[3], modified by a convection term to account for heat transfer to the chamber walls. The use of a 1-D "infinite slab" model for radiation is justified by the high reflectivity of the walls used in the experiment. Temperature-dependent specific heats, thermal conductivities, and absorption coefficients were used, based on the average temperature at a given axial location in the chamber, and the gas was assumed to be in local thermal equilibrium.

The governing equation for the gas temperature in the flow is given by:

$$\rho_o u_o \frac{\partial}{\partial x}(c_p T) = A(x) - R(x) - \frac{4}{d} q''(x),$$

where ρ_0 and u_0 are the inlet gas density and speed, c_p and T are the average specific heat and gas temperature at axial location x, A(x) and R(x) are the volumetric absorption and emission rates of radiation, q" is the convective heat transfer to the wall (per unit wall area), and d is the chamber diameter. The absorption term arises from absorption of both laser radiation and reradiation by the gas:

$$A = \alpha_L I_L + \int_o^\infty d\lambda \alpha_\lambda \int d^3 r' \frac{R_\lambda(r') P_\lambda(r, r')}{4\pi |r - r'|^2}$$

where α_L is the local absorption coefficient at the laser wavelength, I_L is the local laser intensity, α_λ is the spectral absorption coefficient, R_λ is the spectral volumetric radiation, and P(r,r') is the attenuation of radiation from point r to point r':

$$P(r, r') = \exp\left(\frac{s_\lambda(x) - s_\lambda(x')}{|\cos\Theta_{rr'}|} \right),$$

$$s_\lambda(x) = \int_0^x dx' \alpha_\lambda(x') \quad \text{[optical depth to position x]}.$$

The local laser intensity is simply the incident intensity diminished by the absorption to position x: $I_L(x)=I_L(0)\exp(-\alpha_L x)$. The volumetric radiation is given by:

$$R(x)=\int_0^\infty d\lambda R_\lambda(x)$$

where the spectral volumetric radiation is $R_\lambda(x)=\alpha_\lambda(x)B_\lambda(x)$, and $B_\lambda(x)$ is the Planck function:

$$B_\lambda=\frac{2\pi hc^2}{\lambda^5[\exp(hc/\lambda kT)-1]}$$

It is seen that the radiative transport is wholly dependent on the gas absorption coefficient $\alpha_\lambda(x)$. This absorption coefficient was approximated by a discrete band model, using the Edwards Wide-Band Model,[16] characterized by spectral location, integrated intensity, bandwidth, and linewidth parameter. The band parameters for SF_6 were obtained from Ref. 17, and Fig. 25, which also shows the locations and relative strengths of the bands. The temperature dependence of the absorption of SF_6 was taken from Ref. 18 as a power series:

$$\alpha_L(T)=\alpha_{L0}\left\{1+a\left(\frac{T}{T_0}-1\right)+b\left(\frac{T}{T_0}-1\right)^2+c\left(\frac{T}{T_0}-1\right)^3\right\},$$

with α_{L0}=0.18/cm-torr, a=2.3, b=-2.5,c=0.6, T_0=295K. The corresponding Edwards parameters for CO_2 were taken from Ref. 16, and are shown in Fig. 26, and the temperature dependence of the absorption coefficient was also taken as a power series, with coefficients taken from Ref. 19.

The convection heat transfer was determined by using the average of the Nusselt number over the length of the chamber:

$$q''=\frac{\overline{Nu}\cdot k}{d}(T-T_w)$$

Exponential Wide Band Parameters for SF_6

Wavelength, μm	Spectral Location, cm^{-1}	Integrated Intensity, α_o, (cm^{-2} atm^{-1})	Band Width Parameter, ω_o	Line width parameter, β
16.26	615	310	8	0.247
11.5	870	20	38.8	0.0593
10.55	948	~4135	~22	
10.1	991	62	4.88	0.419
6.3	1588	37	19.4	0.266
5.8	1720	17	8.5	0.218

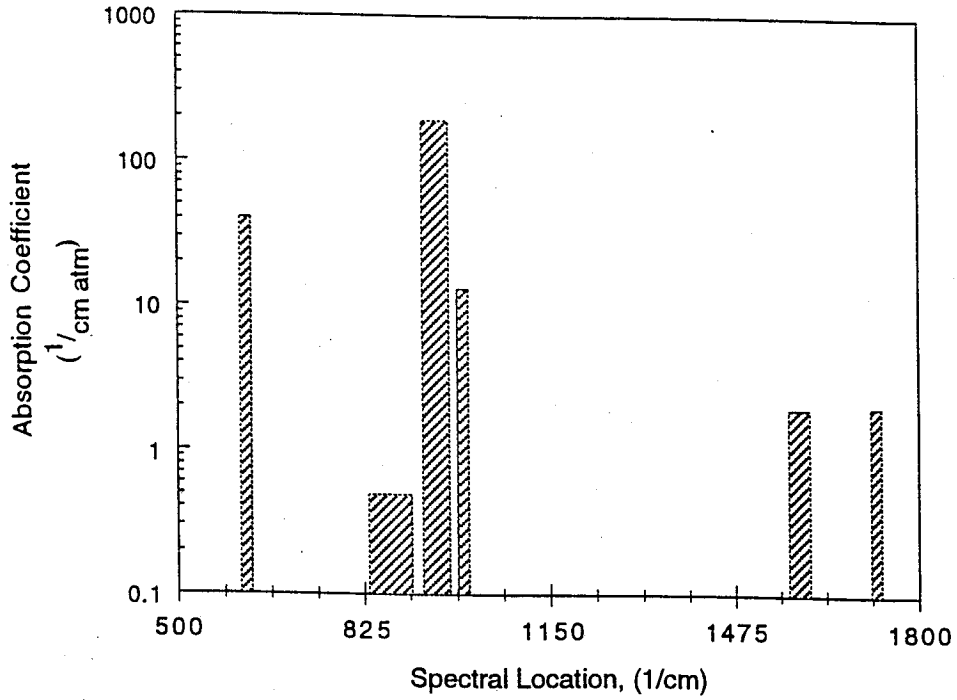

Picket Fence Model for Absorption Spectrum of SF6

Fig. 25 Absorption band parameters and band profile for SF_6.

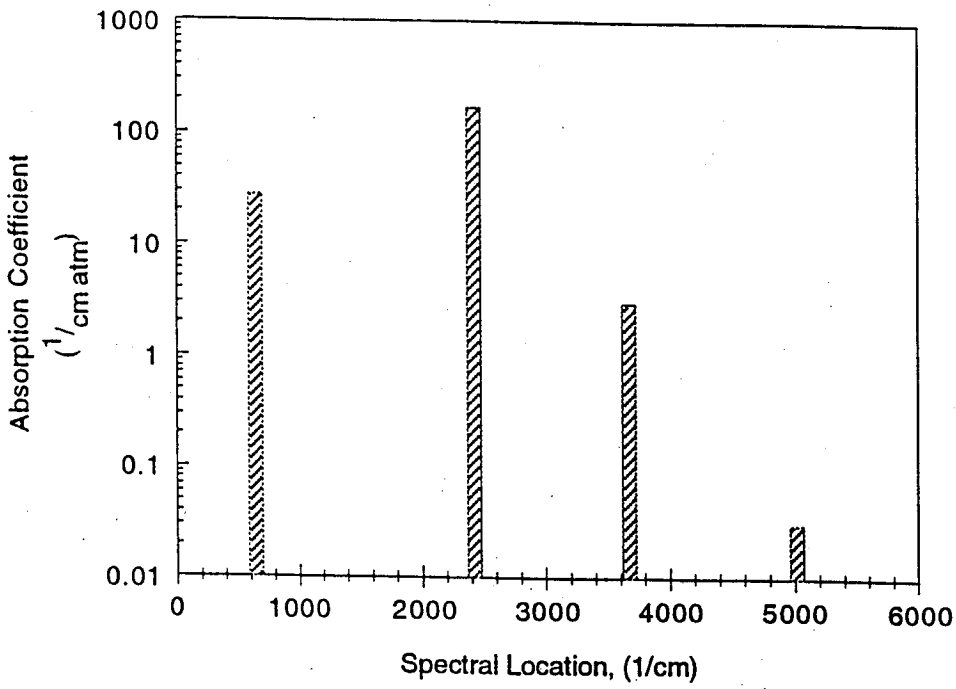

Picket Fence Model for Absorption Spectrum of CO_2

Exponential Wide Band Parameters for CO_2

Wavelength, μm	Spectral Location, cm^{-1}	Integrated Intensity, α_o, (cm^{-2} atm^{-1})	Band Width Parameter, ω_o	Line width parameter, β
15	667	336.87	12.7	0.06157
4.3	2410†	1950.3	11.2	0.24723
2.7	3660	70.29	23.5	0.13341
2.0	5000	1.17	34.5	0.39305

Fig. 26 Absorption band parameters and band profile for CO_2.

where T_W is the local wall temperature, k is the thermal conductivity of the gas, and $\overline{Nu}$ is the Nusselt number averaged over the channel, taking into account the entry length (approximately 3 cm). The Nusselt number in the entry region was obtained from Ref. 20, and in the fully-developed region Nu=4.36. Laminar flow prevailed in this experiment since the Reynolds number was quite low ($Re_D \approx 50$). The average Nusselt number for typical experimental conditions was Nu≈4.9. This method of computing convective heat transfer gave the best correlation with experiment.

The basic heat transfer equation was discretized via use of the band model for radiation, and by dividing the channel into cells of length Δx. The temperature change across cell "i" is then given by:

$$\Delta T_i = \frac{\Delta x}{C_p T(x) \rho_o u_o} \Big\langle \pi Nu \cdot k(T_{w,i} - T_i) + \alpha_L(T_i) I_L e^{-s_{L,i}} + \sum_{bands} \frac{C_{1,\lambda}}{\Delta\lambda} \Big\{ -E_2(s_{L,i}) R(T_i,\lambda) - \frac{1}{2} \sum_{k=0}^{i} \left[R(T_k,\lambda) - R(T_{k-1},\lambda) \right] E_2[s_{\lambda,i} - s_{\lambda,k}] + \frac{1}{2} \sum_{k=i}^{i\max} \left[R(T_k,\lambda) - R(T_{k-1},\lambda) \right] E_2[s_{\lambda,k} - s_{\lambda,i}] \Big\} \Big\rangle,$$

where E_2 is the exponential integral of order 2, and $C_{1,\lambda}$ is the integrated band intensity of band "λ":

$$\int_0^\infty d\lambda B_\lambda = \sum_{bands} C_{1,\lambda} \frac{R(T,\lambda)}{\Delta\lambda}.$$

The quantity $R(T,\lambda)=\sigma T^4 *$(fraction of radiation in band λ). This set of equations was solved by choosing an initial temperature profile, and iterating until the profile approached a stable limit (i.e., sufficiently small deviation from iteration to iteration).

Figure 27 shows the gas temperature profiles at three SF_6 pressures predicted from this analysis, and the expected laser intensity profile in the absorption chamber. These results were

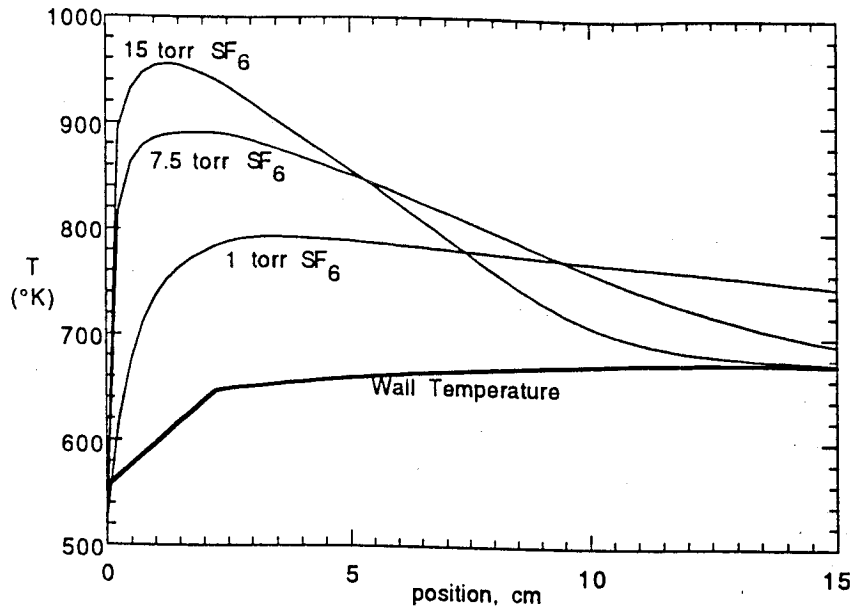

(a)

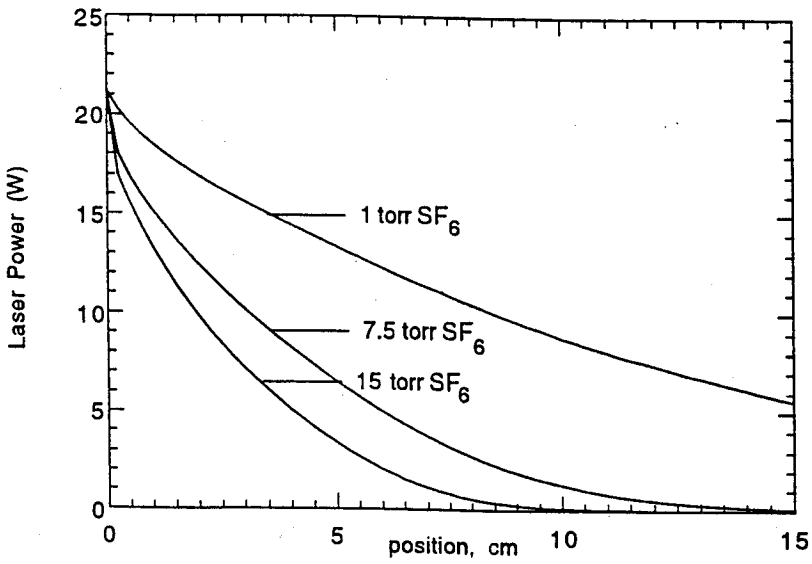

(b)

Fig. 27 Analytical results for (a) gas temperature profile, and (b) intensity profile, in $CO2/SF_6$ gas mixtures at 3 concentrations of SF_6.

computed assuming a laser power of 23 W and a gas flow speed of 1.67 cm/s. As the SF_6 pressure increases, the laser beam is attenuated more rapidly and the gas temperature also rises more rapidly. The peak gas temperature increases with SF_6 pressure, but the temperature falls more rapidly downstream of the peak because the higher temperature and longer region of no radiative heating by the laser leads to higher convection losses to the walls.

c) Experimental results

As a demonstration of heating of a gas by absorption of radiation and a test of the above analysis, the temperature profile of an IR-active gas mixture (CO_2 seeded with SF_6) was measured at SF_6 molar concentrations of 0.28%, 0.56% and 1.5%. The profiles, all taken at a laser power of 23 W and with comparable flow velocities of ≈14.5 cm/sec, are plotted in Fig. 28. These profiles are comparable to those of Fig. 27, and demonstrate the behavior of higher peak temperatures and a greater temperature falloff at increasing concentrations of SF_6.

The *outlet* temperature of a CO_2/SF_6 mixture was also measured as a function of SF_6 concentration, as shown in Fig. 29. This data was all taken at a flow velocity of 14.3 cm/s at a laser power of 21 W. The outlet temperature rises, as expected, with increasing concentration of absorbing gas, and reaches a peak at a concentration of 0.15% by mole. This corresponds to an optical depth for the chamber of approximately 2.0. Thereafter, the outlet temperature decreases monotonically with SF_6 concentration up to concentrations of 1.5%. This data was useful in assessing the basic character of radiative heating by the laser, but did not provide definitive evidence of the effects of radiation trapping, because of the dominance of convective heat transfer at the scale of the absorption chamber.

In order to isolate the effects of radiation trapping from convective heat transfer, a set of temperature measurements were made using both IR-active gas (CO_2/SF_6) and two IR-inactive gases (Ar/SF_6 and N_2/SF_6). The experiments were carried out under similar laser illumination and gas flow conditions, listed in table 2. Although there is some reradiation and trapping in the IR-inactive mixtures, it is very small in comparison with convective heat transfer. Table 3 lists

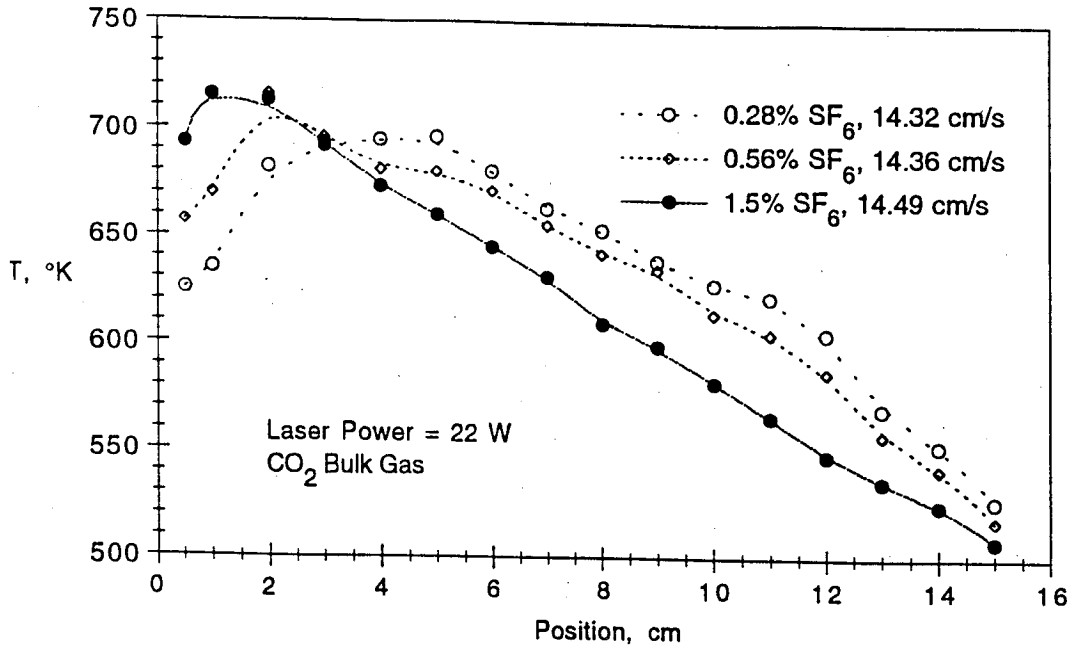

Fig. 28 Measured FGRR gas temperature profiles for CO_2/SF_6 gas mixtures at three SF_6 concentrations.

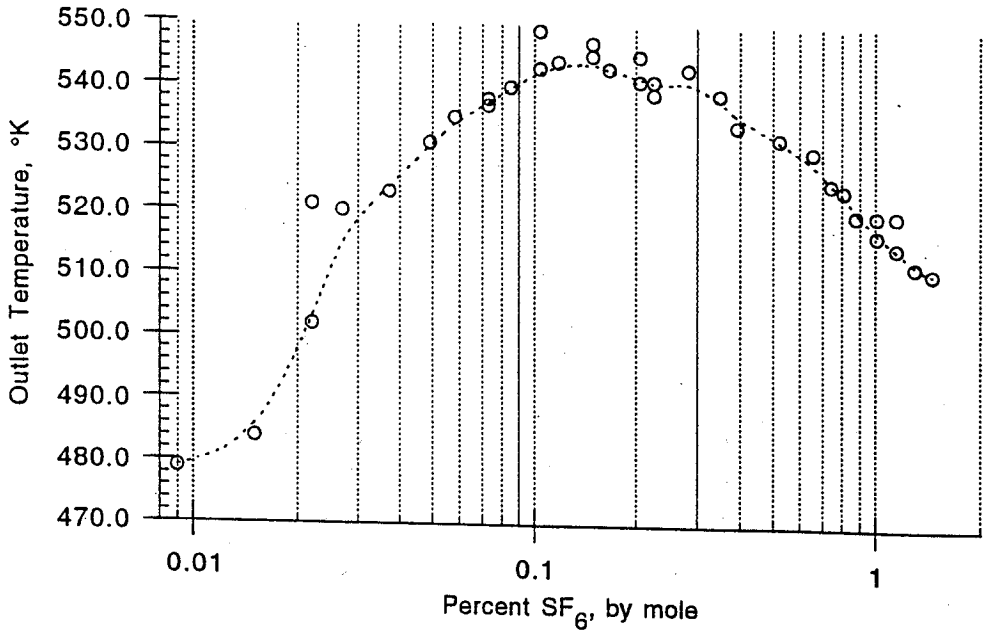

Fig. 29 Variation of CO_2/SF_6 gas outlet temperature with SF_6 concentration.

TABLE 2

Gas flow conditions for radiation trapping measurements.

Bulk Gas	% SF_6, by mole	Flow Speed, U_o (cm/s)	Laser Power, W	Outlet Temp, °K	Peak Temp, °K
CO_2	0.73	2.67	23	721.3	879.3
Ar	0.82	2.73	23.2	762.3	917.6
N_2	1.02	2.55	24	724.9	889.9

TABLE 3

Contributions from CO2 and SF6 bands to gas reradiation.

Wavelength (μm)	Spectral Location (cm^{-1})	% Contribution to total Radiation
CO_2:		
15	667	10.0
4.3	2410	86.4
2.7	3660	1.1
2.0	5000	0.4
	total:	97.9
SF_6:		
16.26	615	0.08
11.5	870	8.62E-03
10.55	948	1.94
10.1	991	0.03
6.3	1588	0.02
5.8	1720	0.01
	total:	2.1

the percentage contribution to gas reradiation in the CO_2/SF_6 mixture, showing that SF_6 only contributes 2%. The Ar/SF_6 and N_2/SF_6 mixtures were thus assumed to have negligible reradiation (and radiation trapping).

The temperature profiles measured for the IR-inactive gases were used to verify (and refine) the analytical model of convective heat transfer, since this is the only means of heat transfer for these mixtures. With this information, the convective part of the heat transfer in the IR-active gas could be accurately modeled and applied to the experiments with CO_2/SF_6 mixtures.

The measured temperature profiles are plotted in Fig. 30, which also plots the theoretical profiles for these mixtures. The theoretical profile that would result for the CO_2/SF_6 mixture *without* radiation trapping is also plotted for comparison. Experimental temperatures are accurate to about ±5 K. It is seen that the experimental and theoretical profiles for all three mixtures agree well, except that the Ar/SF_6 temperatures are somewhat underpredicted by theory. Most striking is that the measured CO_2/SF_6 temperature profile agrees within experimental error with the theoretical profile *including* radiation trapping, but is much different (by > 100K at the outlet) from the predicted profile which neglects trapping (i.e., all reradiation by CO_2 can escape through the entrance window). These results confirm the importance of radiation trapping in establishing the temperature profile of the gas in a flowing-gas radiation receiver, and demonstrate that this effect leads to reduction in energy loss from the receiver.

It should be noted that the above-described experiments already demonstrate the enhanced performance of the FGRR in comparison with a blackbody receiver, both in the cases of IR-active and IR-inactive gases. Defining a receiver efficiency to be 1-(power escaping receiver)/(power entering receiver), a blackbody receiver exposed to the laser flux used in the above experiments would have a receiver efficiency in the range 0.70-0.76, based on a blackbody temperature equal to the average gas temperature, whereas the measured FGRR efficiencies ranged from 0.94 to 0.99 discounting window loss, or 0.84-0.89 including this loss. The power transferred to the

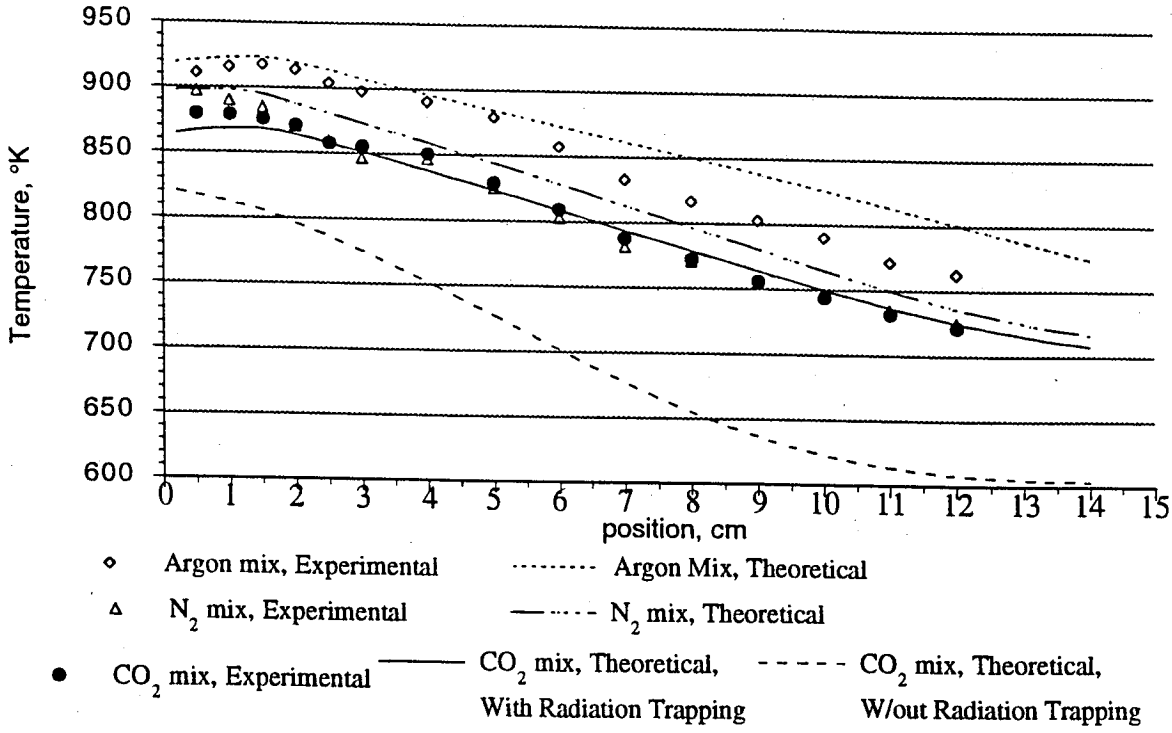

Fig. 30 Experimental and theoretical FGRR temperature profiles for IR-active (CO_2/SF_6) and IR-inactive (N_2/SF_6 and Ar/SF_6) mixtures. Bottom curve neglects radiation trapping in CO_2/SF_6.

FGRR walls was considered "useful" (not lost), as, in fact, it could be employed as part of the heating process (regeneration) for space power or propulsion.

To verify this point, a final series of experiments were carried out to measure the performance of the absorption chamber, modified so that the radiation is absorbed by a solid, and transferred to pure CO_2 by conduction and convection. The performance of this receiver was compared with that of the FGRR using a CO_2/SF_6 mixture as above, but without actively heating the outer wall of the chamber. The FGRR and blackbody receiver configurations are illustrated in Figs. 31a and 31b, respectively. The FGRR used a counterflow configuration, whereby the gas was preheated by the inner chamber wall. The blackbody receiver used a small piece of stainless steel wool, coated with a black, flame-resistant paint to intercept and absorb the incident radiation. Flow velocities for both receivers were varied in the range 8-21 cm/sec, and the outlet gas temperature was measured.

For comparison purposes the receiver efficiency was taken to be the enthalpy gain of the gas divided by the incident laser power, with the power losses at the window discounted for the blackbody receiver. Figure 32 plots the results as efficiency vs. flow rate. It is seen that even in this conservative comparison, the FGRR has a significantly higher efficiency than a blackbody receiver, due to reduced reradiation losses. This advantage is expected to be even greater at higher radiation fluxes and higher gas temperatures.

CONCLUSION

These experiments confirm for the first time that radiation trapping inherent in the operation of the flowing gas radiation receiver leads to reduced radiation losses in comparison with conventional solid-surface receivers. The FGRR has the capability of producing working fluid temperatures far beyond those attainable by conventional receivers, while maintaining high receiver efficiency and is thus of considerable interest for solar-driven space power and propulsion applications. Future development of the FGRR approach should be directed at demonstration of

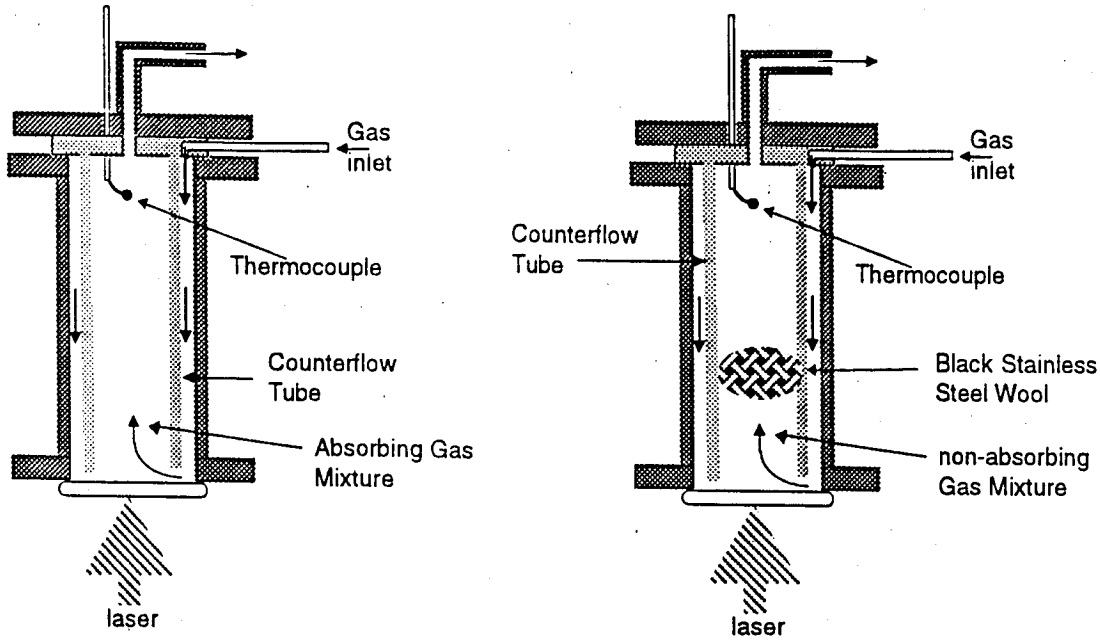

Fig. 31 Receiver configurations for comparing FGRR and blackbody efficiencies

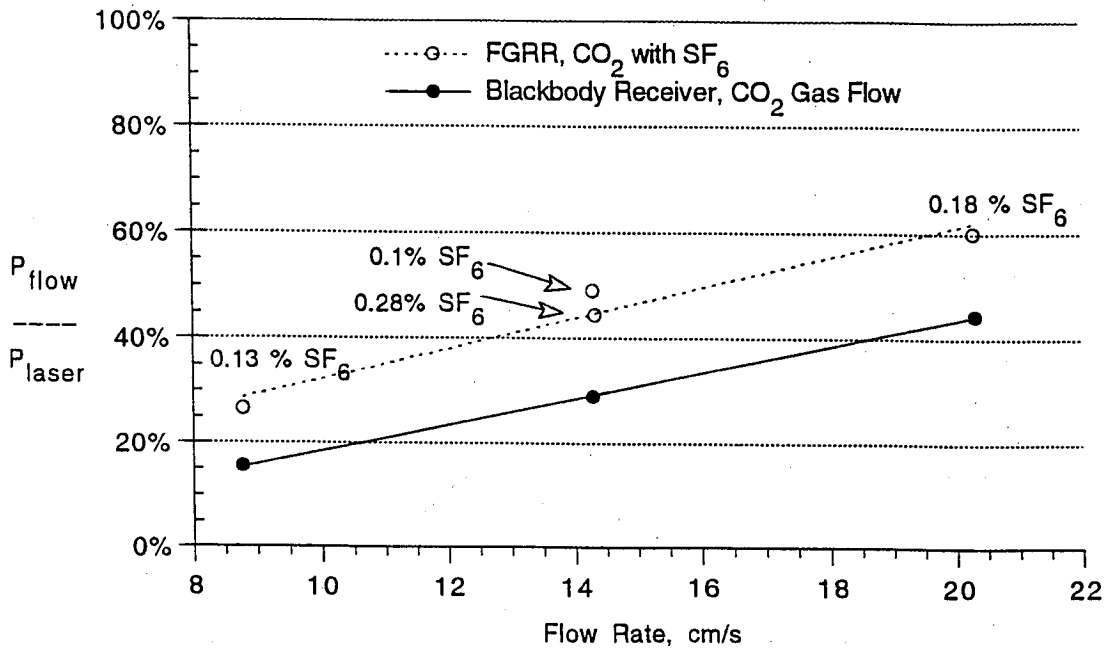

Fig. 32 Comparison of receiver efficiency vs flow rate for FGRR and blackbody receivers.

its performance at high radiation fluxes, using broadband seedants for effective coupling to the solar spectrum, and at measuring the ISP and thrust levels attainable in propulsion applications.

REFERENCES - CHAPTER II

1. A.T. Mattick, A. Hertzberg, R. Decher, and C.V. Lau, "High-temperature solar photon engines," *J. Energy* **3**, 30-39 (1979).

2. C. Seippel, "Pressure exchanger", US Patent 2399394 (1946).

3. A.T. Mattick, "Coaxial radiative and convective heat transfer in gray and nongray gases," *J. Quant. Spectrosc. Radiat. Transfer* **24**, 323-334 (1980).

4. D. Rault, "Radiation energy receiver for high performance energy cycles," Ph.D. Dissertation, University of Washington (1980).

5. D. Rault and A. Hertzberg, "Radiative energy receiver for high performance energy conversion cycles," *Proc. IECEC*, 113 (1982).

6. D. Rault and A. Hertzberg, "Radiative energy receiver for laser and solar propulsion systems," AIAA Paper 83-1207, AIAA 19th Joint Propulsion Conf., Seattle, WA, June 27-29 (1983).

7. "Advanced solar-propelled cargo spacecraft for Mars missions," USRA Advanced Design Program, Univ. of Washington (1989).

8. A.T. Mattick and K.A. McFall, "Efficient space propulsion and power using a high-temperature, gaseous radiation receiver," Paper AIAA 90-1615, AIAA 21st Fluid Dynamics, Plasma Dynamics and Lasers Conference, Seattle, WA, June 18-20 (1990).

9. K.A. McFall and A.T. Mattick, "Two dimensional analysis of a high temperature gaseous radiation receiver," Paper AIAA 92-3215, AIAA 28th Joint Propulsion Conference, Nashville, TN, July 6-8 (1992).

10. K.A. McFall, "Radiative heat transfer in the high-temperature flowing gas radiation receiver," Ph.D. Dissertation, Univ. of Washington (1991).

11. S.T. Thynell and C.L. Merkle, "Analysis of volumetric absorption of solar energy and its interaction with radiation," *J. Heat Transfer* **111**, 1006-1014 (1989).

12. R.P. Hoyt, "Experimental studies of radiation trapping in the flowing gas radiation receiver,", M.S. Thesis, Univ. of Washington (1992).

13. P. Kubat and J. Pola, "Spatial temperature distribution in CW CO2 laser photosensitization reactions," *Coll. Czech. Chem. Commun* **49**, 1354-1359 (1984).

14. S. Ruschin and S.H. Bauer, "Oscillating convective effects in SF6-Ar laser heated mixtures," *J. Phys. Chem.* **88**, 5042-48 (1984).

15. H.F. Nelson and E.A. Eiswirth, "CO2 laser absorption in SF6-air boundary layers," *J. Thermophys.* **3**, p. 353 (1990).

16. D.K. Edwards, "Molecular gas band radiation," in *Advances in Heat Transfer* **12**, p. 145 (1976).

17. S. Reilly et. al., "Infrared radiation of SF6 and its application to gas-filled double-pane windows," *Experimental Heat Transfer* **3**, 65-80 (1990); A. Nowak and J.L. Lyman, "The temperature-dependent absorption spectrum of the ν3 band of SF6 at 10.6 μm," J. *Quant. Spectrosc. Radiat. Transfer* **15**, 945-961 (1975).

18. S.E. Pankratov et. al., "Temperature dependence of absorption cross sections of polyatomic gases in the interval 900-1100 cm^{-1}," *Khim Vys Energ.* **24**, 464-466 (1989).

19. Robinson and Garand, "Extended high temperature measurements of absorption at 10.4 μm in CO_2," *Appl. Optics* **28** (1989).

20. F.P. Incropera and D.P. Dewitt, *Fundamentals of Heat and Mass Transfer*, John Wiley and Sons, (1981).